A one-electron model for the aqueous electron that includes many-body electron-water polarization: Bulk equilibrium structure, vertical electron binding energy, and optical absorption spectrum

Leif D. Jacobson and John M. Herbert[a)]
Department of Chemistry, The Ohio State University, Columbus, Ohio 43210, USA

(Received 1 July 2010; accepted 28 August 2010; published online 19 October 2010)

Previously, we reported an electron-water pseudopotential designed to be used in conjunction with a polarizable water model, in order to describe the hydrated electron [L. D. Jacobson *et al.*, J. Chem. Phys. **130**, 124115 (2009)]. Subsequently, we found this model to be inadequate for the aqueous electron in bulk water, and here we report a reparametrization of the model. Unlike the previous model, the current version is not fit directly to any observables; rather, we use an *ab initio* exchange-correlation potential, along with a repulsive potential that is fit to reproduce the density maximum of the excess electron's wave function within the static-exchange approximation. The new parametrization performs at least as well as the previous model, as compared to *ab initio* benchmarks for $(H_2O)_n^-$ clusters, and also predicts reasonable values for the diffusion coefficient, radius of gyration, and absorption maximum of the bulk species. The new model predicts a vertical electron binding energy of 3.7 eV in bulk water, which is 1.4 eV smaller than the value obtained using nonpolarizable models; the difference represents the solvent's electronic reorganization energy following electron detachment. We find that the electron's first solvation shell is quite loose, which may be responsible for the electron's large, positive entropy of hydration. Many-body polarization alters the electronic absorption line shape in a qualitative way, giving rise to a high-energy tail that is observed experimentally but is absent in previous simulations. In our model, this feature arises from spatially diffuse excited states that are bound only by electronic reorganization (i.e., solvent polarization) following electronic excitation. © *2010 American Institute of Physics*.
[doi:10.1063/1.3490479]

I. INTRODUCTION

Since its absorption spectrum was first observed in 1962,[1,2] there have been numerous experimental[3–32] and theoretical studies[33–65] focused on elucidating the structure, dynamics, and spectroscopy of the aqueous electron (e_{aq}^-) in bulk water, as well as finite $(H_2O)_n^-$ cluster anions. The hydrated electron is a prototypical system for studying the interplay between quantum mechanics, which is required to describe the unpaired electron, and classical mechanics, which is necessary to sample over solvent configurations or cluster morphologies. Despite extensive study, however, agreement between theory and experiment—regarding some of the most basic structural and spectroscopic properties of these systems—is still lacking.

Extrapolation of the vertical electron binding energies (VEBEs) for $(H_2O)_n^-$ cluster anions suggests a value of ≈3.4 eV for the VEBE of the aqueous electron,[7,66] consistent with several recent direct measurements of the VEBE for e_{aq}^- using liquid microjets.[30–32] However, recent simulations using one-electron pseudopotential models suggest that the cluster photoelectron experiments do not actually probe "internal" (cavity-bound) states of the excess electron, but rather surface-bound states with no bulk analog.[48,53] This interpretation remains controversial,[67–69] and the cluster size at which the electron internalizes remains a topic of contemporary interest.

The optical absorption spectrum is the primary experimental handle for e_{aq}^- in bulk solution, yet quantitative reproduction of this spectrum by theoretical means has proven elusive. Simulations based on a one-electron pseudopotential model developed recently by Turi and Borgis[47] (TB) reproduce the absorption maximum to within ~0.2 eV,[47,64] but so far none of the different one-electron models that have been developed over the years[35,40,41,46,47,54] reproduces the asymmetric Lorentzian tail that is observed on the blue edge of the spectrum.[66,70–73]

The solvation environment of the bulk species is also under discussion. Long ago, Kevan[3,4] proposed a hexavalent coordination motif, based upon spin echo measurements in aqueous glasses at $T=77$ K. Shkrob[61] recently provided theoretical support for this interpretation, based upon *ab initio* calculations of hyperfine coupling constants in small $(H_2O)_n^-$ clusters. However, the aforementioned TB model potential affords a tetravalent structure at $T=300$ K.[47] Very recently, Larsen *et al.*[65] suggested, based upon a different one-electron model, that the e_{aq}^- wave function is not really "coordinated" in the same sense as atomic ions such as Br^- or I^-, but is instead delocalized over a large number of water molecules, on which it exerts only a weak orientational influence. Further complicating the matter are vibrational spectra of

a)Electronic mail: herbert@chemistry.ohio-state.edu.

$(H_2O)_n^-$ clusters that suggest the presence of a so-called double acceptor ("AA") electron electron binding motif[16–18] in clusters as large as $n=50$,[23] whereas resonance Raman spectra of the bulk species are interpreted as arising from a coordination motif that involves only one hydrogen atom per water molecule.[15]

Motivated by these outstanding issues, we decided to revisit the most basic structural, spectroscopic, and dynamical aspects of the hydrated electron, using a one-electron model that is built upon a sophisticated and accurate water force field. In practice, this means a polarizable force field, whereas most previous one-electron models for e_{aq}^- have employed fairly rudimentary water models, such as the "simple point charge" (SPC) model.[74,75] We expect that a polarizable model will better describe the relative energies of distorted hydrogen-bonding networks that are stabilized by the excess electron, but are highly unfavorable in neutral water.[76,77] In addition, we wish to determine the extent to which a self-consistent treatment of many-body electron-water polarization is qualitatively important. Along these lines, we note that cavity-bound $(H_2O)_n^-$ isomers are characterized by a much larger number of significant electron-H_2O interactions, as compared to surface-bound isomers.[78] As such, one might expect very different polarization energies for surface- versus cavity-bound electrons.

Previously,[79] we reported an electron-water pseudopotential designed for use with the "AMOEBA" polarizable water model.[80,81] In the discussion that follows, this one-electron model for e_{aq}^- is termed "polarizable electron-water potential, version 1" (PEWP-1). Compared to the nonpolarizable TB model,[47] which has been used extensively in recent simulations,[47–53,63] PEWP-1 affords significantly better agreement with *ab initio* benchmarks for both VEBEs and relative isomer energies of $(H_2O)_n^-$ clusters.[79] When used to simulate e_{aq}^- in bulk solution, however, we found that PEWP-1 predicts a diffuse ground-state electronic wave function that penetrates throughout the water network, rather than forming a proper cavity.[77] As a result, PEWP-1 predicts an unrealistically fast diffusion coefficient of $\gtrsim 1.0$ Å^2/ps at 300 K, as compared to an experimental value of 0.51 Å^2/ps.[6] Given the compelling experimental evidence for electron localization in polar fluids,[3,4,82] plus the fact that *ab initio* calculations strongly suggest cavity formation in hydrated-electron systems,[58,64,83] we rejected this model and decided to revisit the parametrization of the electron-water pseudopotential. The largest difference between our previous parametrization and the one reported here, the latter of which we shall call PEWP-2, is that the new potential is much more repulsive in the core molecular region. This difference alone facilities cavity formation.

In this work we reparametrize our model on the basis of the static exchange (SE) approximation.[84–87] Unlike previous SE treatments, however, we use density functional theory (DFT) to provide an electron-water exchange-correlation potential, rather than relying on Hartree–Fock theory for this purpose. After construction of an exchange-correlation potential, we fit a repulsive potential in order to reproduce the density maximum of the lowest unoccupied molecular orbital (LUMO) near the core molecular region. As compared to the original parametrization (PEWP-1), this new model (PEWP-2) affords even better agreement with *ab initio* benchmarks for $(H_2O)_n^-$ clusters. Application of PEWP-2 to the bulk aqueous electron reveals that the description of electronic relaxation upon electron detachment is crucial for obtaining a reasonable bulk binding energy. Most interestingly, the inclusion of electron-water polarization not only provides an accurate prediction of the optical absorption maximum, but for the first time affords a significant "blue tail" in the spectrum, vastly improving the agreement with the experimental line shape, as compared to all previous one-electron models.

II. REPARAMETRIZATION OF THE MODEL POTENTIAL

A. Motivation

In order to construct a scalar potential for the electron-water interaction, we follow the procedure of Smallwood *et al.*,[88] which provides a computationally exact way to solve for the Phillips–Kleinman[89] pseudo-wave function. Although this procedure was developed in the context of Hartree–Fock (HF) theory, one can easily replace the HF exchange operator with the exchange-correlation operator defined by any Kohn–Sham density functional, and thereby obtain a potential that includes dynamical correlation, provided that one accepts that the Kohn–Sham molecular orbitals (MOs) are suitable replacements for the HF MOs. The problem with using traditional DFT for the hydrated electron is that self-interaction error causes widely-used functionals such as B3LYP and BLYP tend to overbind the unpaired electron by a significant amount.[83] Recently-developed "long-range corrected" (LRC) density functionals, however, are asymptotically free of self-interaction error, and the LRC-μBOP functional[90,91] has recently been shown to provide extremely accurate VEBEs in $(H_2O)_n^-$ clusters.[79,92] Presumably, this is because the singly occupied MO (SOMO) mostly occupies a region of space apart from the valence MOs, and the LRC procedure therefore eliminates self-interaction error associated with the SOMO.

At the outset, we should clarify that we expect any pseudopotential to be semiquantitative at best, due to a neglect of many-electron contributions to the wave function, which appear to be necessary in order to explain certain aspects of the spectroscopy of e_{aq}^-. All-electron calculations in $(H_2O)_n^-$ clusters indicate that $\sim$10%–20% of the spin density resides on H_2O molecules, which provides an explanation for observed vibrational red shifts[59] and hyperfine coupling constants.[61] In addition, the total oscillator strength associated with the optical spectrum of e_{aq}^- is $\sim$1.1,[29] indicating that the electronic excitations contain a small amount of many-electron character. (Because the excited states obtained from time-dependent DFT calculations clearly resemble particle-in-a-box eigenstates,[64] however, we expect that many-electron character plays only a minor role in the excitation spectrum.)

In view of these facts, our main aim is to study the extent to which polarization is qualitatively important in de-

scribing the features of $(H_2O)_n^-$ clusters and bulk e_{aq}^-, using a model that is tractable enough to facilitate adequate statistical sampling. At the same time, we do wish to make contact with photoelectron data and to infer relationships between cluster spectroscopy and bulk measurements, both of which demand an accurate treatment of VEBEs. Furthermore, the ongoing debate regarding surface states versus cavity states in $(H_2O)_n^-$ clusters is, at its core, a debate over extrapolations to the bulk limit, so we desire a model that can also reproduce bulk properties.

The model constructed herein is empirical in nature; we use the SE approximation as a guide to constructing a potential, but not to *derive* quantitative interaction terms. That said, we do not fit this model directly to any measured or computed observables, so to the extent that the model successfully reproduces observables, it is reasonable to conclude that much of the basic physics has been described successfully.

B. The static-exchange approximation

To date, most electron-water pseudopotentials are either extremely heuristic in nature, which is inconsistent with our goal of achieving at least a semiquantitative description of e_{aq}^- and $(H_2O)_n^-$ spectroscopy, or else are based upon the SE approximation.[84–87] Within this approximation, one considers the interaction of an excess electron with the ground-state wave function of an isolated molecule, in our case, H_2O. The H_2O^- wave function, $|\Psi\rangle$, is taken to be an antisymmetrized product of the excess-electron orbital, $|\psi\rangle$, and the frozen MOs from a (neutral) H_2O calculation, $|\psi_i\rangle$. This leads to a one-electron eigenvalue equation for the excess electron,[84–86]

$$\hat{H}_{SE}|\Psi\rangle = (\hat{T} + V_n + V_H + \hat{V}_{xc})|\Psi\rangle = \varepsilon|\Psi\rangle. \tag{1}$$

Here, $\hat{T}$ is the kinetic energy operator, V_n is the electron-nuclear Coulomb interaction, V_H is the electronic Coulomb (Hartree) energy, and $\hat{V}_{xc}$ is the (nonlocal) exchange-correlation operator. The quantities V_H and $\hat{V}_{xc}$ are identical to the Coulomb and exchange (or exchange-correlation) operators in a HF (or Kohn–Sham DFT) calculation of H_2O, hence the highest occupied MO in the SE approximation is the LUMO in the HF or DFT calculation. Inclusion of a DFT exchange-correlation component in Eq. (1) is a novel feature of the present treatment.

Although Eq. (1) is a one-electron eigenvalue equation, construction of $\hat{H}_{SE}$ requires the H_2O MOs. This dependence must be removed in order to obtain a scalar potential $V(\vec{r})$ that can be readily evaluated and fit to some analytical expression, thus converting Eq. (1) into a simple one-electron eigenvalue equation, $(\hat{T}+V)|\Psi\rangle=\varepsilon|\Psi\rangle$.

Following Schnitker and Rossky,[85] we write the actual SE wave function, $|\psi\rangle$, as a linear combination of a nodeless wave function, $|\phi\rangle$, that is asymptotically correct but lacks oscillations in the core molecular region, along with a residual that is expanded in terms of the MOs, $|\psi_i\rangle$, from a calculation on an isolated H_2O molecule,

$$|\psi\rangle = |\phi\rangle + \sum_i^{N_{occ}} c_i|\psi_i\rangle. \tag{2}$$

Inserting Eq. (2) into Eq. (1) affords an eigenvalue equation for the nodeless wave function,[85]

$$\left(\hat{H}_{SE} + \sum_i^{N_{occ}} (\varepsilon - \varepsilon_i)|\psi_i\rangle\langle\psi_i|\right)|\phi\rangle = \varepsilon|\phi\rangle. \tag{3}$$

The second term in parenthesis in Eq. (3) is an operator that forces $|\phi\rangle$ to remain outside of the core (H_2O) region, preventing variational collapse. One may express the action of this operator on $|\phi\rangle$ using a (scalar) repulsive potential

$$V_{rep}(\vec{r}) = \sum_i^{N_{occ}} \frac{(\varepsilon - \varepsilon_i)\psi_i(\vec{r})\langle\psi_i|\phi\rangle}{\phi(\vec{r})}, \tag{4}$$

but this potential then depends upon the nodeless pseudo-wave function itself.

To eliminate this dependence, Schnitker and Rossky make two subsequent approximations:[85] first, that the excess electron is weakly bound ($|\varepsilon| \ll |\varepsilon_i|$), and second, that the nodeless function $|\phi\rangle$ is not only smooth but is constant in the core region. Although the latter assumption is somewhat dubious, without it the nodeless function is not uniquely defined by Eq. (3).[88] Recently, Smallwood *et al.*[88] showed that this ambiguity can be removed (and the assumption that $|\phi\rangle$ is constant in the core region can be avoided) by supplying an additional constraint. Following those authors, we choose this constraint to be that $\langle\phi|\hat{T}|\phi\rangle/\langle\phi|\phi\rangle$ should be minimized. This requirement leads to an iterative recipe for calculating the nodeless pseudo-wave function,[88]

$$|\phi\rangle = |\psi\rangle + \sum_i^{N_{occ}} \frac{\langle\psi_i|\hat{T}|\phi\rangle}{\langle\phi|\hat{T}|\phi\rangle}|\psi_i\rangle. \tag{5}$$

Once $|\phi\rangle$ is known, one can always define an orbital-dependent scalar potential

$$v[\phi](\vec{r}) = \frac{\langle\vec{r}|\hat{v}|\phi\rangle}{\phi(\vec{r})} \tag{6}$$

for any operator $\hat{v}$. [In fact, Eq. (4) is just a special case of Eq. (6).] Construction of this potential requires the H_2O MOs, but once $v[\phi](\vec{r})$ is determined, it can be fit to some analytic form for convenient evaluation. In practice, we will use Eq. (6) to obtain a local potential for exchange and correlation ($\hat{v}=\hat{V}_{xc}$). Note also that since the MOs $|\psi_i\rangle$ used to construct this potential are frozen, polarization is not included in this potential. Polarization is sometimes grafted onto the SE approximation, in the form of a two-body polarization potential of the form

$$V_{pol}(r) = -\frac{\alpha}{2(r^2 + C)^2}, \tag{7}$$

where α is the isotropic polarizability of H_2O and C is a constant.[33,47,85,87] In the present work, *many-body* polarization is incorporated self-consistently, via a polarizable water model from which an electron-water polarization potential arises in a natural way, and from which the two-body poten-

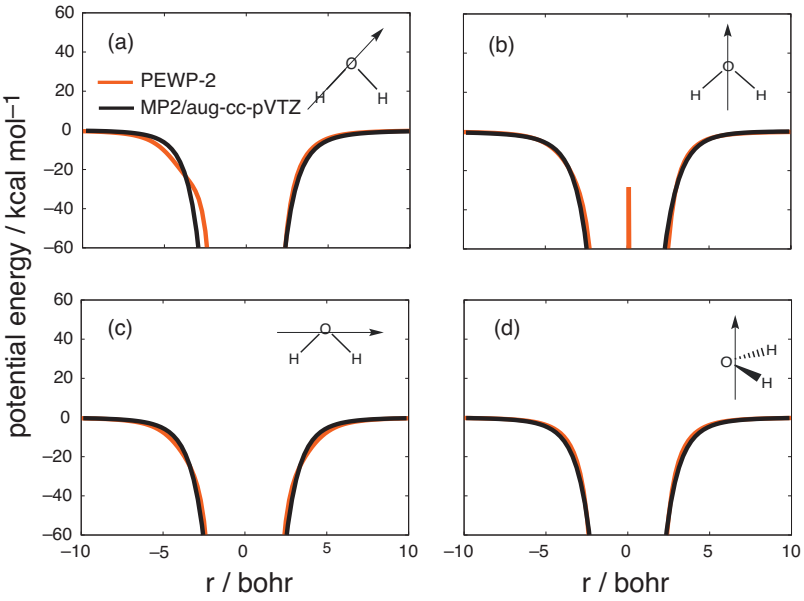

FIG. 1. Calculated MP2 polarization potential as compared to the fit that is used to obtain Coulomb damping parameters. The origin of the coordinate system is the H_2O center of mass, except in panel (a), where the origin is the oxygen atom.

tial in Eq. (7) can be obtained based on well-defined approximations.[79]

Electrostatic interactions between the electron and the water molecules are destined to be replaced by electron-multipole interactions, where the multipoles come from the water force field. Inclusion of the exact SE potentials V_n and V_H from Eq. (1) would double-count these interactions, thus we allow the force field alone to represent the electrostatic parts of the electron-water interaction. The nonelectrostatic components of the interaction, which include Pauli repulsion and exchange-correlation effects, are represented in the form of a potential $V_{\text{rep}}+V_{\text{xc}}$, where V_{xc} comes from Eq. (6) as described above, and V_{rep} is a repulsive potential that prevents collapse of the wave function. Fundamentally, V_{rep} arises from orthogonality; its construction is discussed in Sec. II D.

C. Electrostatic interactions

Electrostatics and polarization are handled in the same way as in our earlier work,[79] to which the reader is referred for details. The essential features are summarized in this section. Let V^{MM} denote all of the intramolecular and water-water interaction terms contained within the AMOEBA force field. Within AMOEBA, electrostatic interactions are represented in terms of permanent charges, dipoles, and quadrupoles, along with inducible dipoles, and we denote the electron's interactions with the permanent and the induced multipoles as $V_{\text{perm}}^{\text{elec-water}}$ and $V_{\text{pol}}^{\text{elec-water}}$, respectively. The full interaction potential is then

$$V^{\text{elec-water}} = V^{\text{MM}} + V_{\text{perm}}^{\text{elec-water}} + V_{\text{pol}}^{\text{elec-water}} + V_{\text{xc}}^{\text{elec-water}} + V_{\text{rep}}^{\text{elec-water}}, \tag{8}$$

where the final two terms come from the pseudopotential. (Fitting of these two terms is discussed in Sec. II D.) Induced dipoles on the water molecules are determined using the total electric field, which contains contributions from the water molecules and from the electronic wave function.[79]

Polarizable force fields based upon induced dipoles must utilize a damped Coulomb operator that is finite as $r\to 0$, in order to avoid a "polarization catastrophe."[93] The water-water interactions within AMOEBA already employ such an operator,[80] which we do not modify here. For the electron-water electrostatic interactions, we use the modified Coulomb potential[79]

$$t_{\text{elec},i} = \frac{\text{erf}(a_i r_{\text{elec},i})}{r_{\text{elec},i}}, \tag{9}$$

where a_i is one of two damping parameters (i=O or H), and $r_{\text{elec},i}$ is the electron-multipole distance. (Technically, $t_{\text{elec},i}$ is the modified Coulomb operator for electron-monopole interactions; analogous quantities for higher-order multipoles are obtained by differentiating $t_{\text{elec},i}$.[79]) This same damped Coulomb operator is used to calculate the wave function's contribution to the electric field.

There is no *a priori* reason why the permanent and induced electrostatic interactions should require the same damping parameters a_i, and our model uses different parameters for each. The damping parameters a_{O} and a_{H} for the electron/induced dipole interactions ($V_{\text{pol}}^{\text{elec-water}}$) are obtained from a fit to an *ab initio* polarization potential for H_2O, calculated at the level of second-order Møller–Plesset perturbation theory (MP2), as follows. We first perform a MP2 calculation on isolated H_2O, then use these MOs as the starting point for a calculation that includes a single $-e$ point charge. The MP2 polarization energy is calculated, as a function of the position of this point charge, and includes both the energy decrease that accompanies orbital relaxation in the presence of the point charge, plus the change in the MP2 correlation energy between the isolated H_2O calculation and the calculation in the presence of the point charge. The parameters a_{O} and a_{H} are then fit to reproduce this polarization potential along each of the four one-dimensional cuts shown in Fig. 1. Since we will ultimately add to this a potential that is quite repulsive in the core molecular region, it is not necessary to obtain an extremely accurate fit for the attractive parts of the potential where r is small; only the region where

$r \gtrsim 3$ bohr is relevant. The fits shown in Fig. 1 are quite good in the relevant region.

D. Repulsive potential and fitting parameters

In order to construct a local potential of the form given in Eq. (6), we first solve Eq. (5) for the nodeless pseudo-wave function, $|\phi\rangle$, using an initial guess corresponding to the LUMO of H_2O. Once a self-consistent solution has been determined, we construct a scalar potential for exchange and correlation by setting $\hat{v}=\hat{V}_{xc}$ in Eq. (6), using the LRC-μBOP functional[90,91] to define $\hat{V}_{xc}$. Alternative density functionals such as LRC-ωPBEOP that afford similar VEBEs yield similar results for the exchange-correlation potential, but the pseudopotentials obtained using functionals that strongly overbind the electron (e.g., B3LYP) are notably different.

To this exchange-correlation potential we must add a repulsive potential, whose physical origin is the orthogonality requirement between the excess-electron MO and the core H_2O MOs. In principle, one could construct a repulsive potential using the expression [cf. Eq. (4)]

$$\hat{V}_{rep} = \sum_{i}^{N_{occ}} (\varepsilon - \varepsilon_i)|\psi_i\rangle\langle\psi_i|, \tag{10}$$

but our attempts to utilize this expression directly were not successful, as the resulting potential is far too repulsive in the core molecular region. In our view, Eq. (10) produces a potential that is much too repulsive for use in conjunction with damped electrostatics, which attenuate the attractive interactions at short range. In parametrizing our previous model, PEWP-1,[79] we drastically scaled down this repulsive potential using a scaling parameter that was fit to reproduce *ab initio* VEBE benchmarks for $(H_2O)_n^-$ clusters; a dramatic scaling of the repulsive potential was also used by Wang and Jordan[94] to develop a different electron-water pseudopotential. Evidently, the Coulomb attenuation in Eq. (9) can compensate for this scaling, because PEWP-1 affords fairly accurate VEBEs across a wide range of energies.[79] When applied to the condensed phase, however, PEWP-1 fails to localize the electron into a cavity and predicts a diffusion coefficient that is too large by at least a factor of 2. We interpret these observations evidence that the repulsive potential has been reduced too much.

As an alternative to Eq. (10), we fit a repulsive potential, as well as damping parameters a_O and a_H for the interaction between the electron and the H_2O permanent multipoles ($V_{perm}^{elec\text{-}water}$). The two damping parameters are fit in order to reproduce the density maximum of the pseudo-wave function confined to the region of the molecule. While we do not directly fit to any VEBEs *per se*, in the final step of this procedure we do reject any fits that do not reproduce *ab initio* VEBEs to within ~0.1 eV.

Calculations to determine the pseudo-wave function utilize a Gaussian basis set that we call "aug-cc-pVQZ+diff−pol". The "+diff" indicates we have added diffuse *s* and *p* functions to each hydrogen atom, with exponents of 0.002 953 75 and 0.0106 bohr^{-2}, respectively; the "−pol" indicates we have removed all *g* and higher angular momentum functions. A single water molecule does not bind an extra electron, so "convergence" of the basis set cannot be achieved with respect to the excess-electron distribution, which is ultimately bound only by the compactness of the basis set. However, the aforementioned basis set should give a good representation of the H_2O density, while being diffuse enough to describe the excess electron distribution in the immediate vicinity of the molecule, which is the chemically significant region. Calculation of the pseudo-wave function was performed using a locally modified version of Q-CHEM.[95]

The exchange-correlation potential obtained from Eq. (6) is computed on a grid of points and then fit to an analytic form consisting of a sum of Gaussian functions centered on the molecular mechanics (MM) atoms,

$$V_{xc}^{elec\text{-}water}(\vec{r}) = \sum_i C_i \exp(-z_i|\vec{r}-\vec{r}_i|^2). \tag{11}$$

A good fit was obtained using a single Gaussian function on the oxygen atom and three Gaussians on each hydrogen atom. (All fitting parameters are provided in the supplementary material.[96]) Figure 2 plots the fitted potential along four one-dimensional slices. As mentioned above, it is only necessary to obtain a good fit to the attractive parts of the exchange-correlation potential in regions where $r \gtrsim 3$ bohr, and our fit is quite reasonable in these regions.

We construct repulsive potentials centered on each MM atom, of the form

$$V_{rep}^{elec,i}(\vec{r}) = \frac{B_1^i}{r_{elec,i}}[\mathrm{erf}(B_2^i r_{elec,i}) - \mathrm{erf}(B_3^i, r_{elec,i})], \tag{12}$$

where i=O or H, and $r_{elec,i}=|\vec{r}-\vec{r}_i|$. (The total repulsive potential is the sum of the three atom-centered potentials.) Equation (12) is the same functional form used by Turi and Borgis[47] to obtain a scalar potential that reproduces the SE pseudo-wave function, neglecting exchange and correlation interactions. Following those authors, we apply a confining potential of the form $V_{conf}=k(x^8+y^8+z^8)$, with $k=5\times10^{-7}E_h$, which keeps the (unbound) excess electron near the core region. This confining potential is only employed in order to fit the pseudo-wave function, and not when fitting to the exchange-correlation potential described above. We believe that applying a confining potential is reasonable in that it should mimic the behavior of the excess electron in a high density environment,[97] and hence provide guidance for the fitting of the repulsive potential.

Figure 3 shows the density of the excess electron, $|\psi|^2$, calculated using various methods. The H_2O LUMOs computed at both the HF and LRC-μBOP levels are shown, as are the corresponding SE pseudo-wave functions. Also shown are the ground-state wave functions obtained using the PEWP-1, PEWP-2, and TB model potentials, the latter having been fit to reproduce the HF pseudo-wave function. Several important observations can be made from Fig. 3. Comparing the LUMOs to the SE pseudo-wave functions, we observe that the latter are indeed asymptotically correct while lacking the large amplitude oscillation in the molecular core. The position of the density maximum in the LUMO, which is similar at both the HF and LRC-μBOP levels of

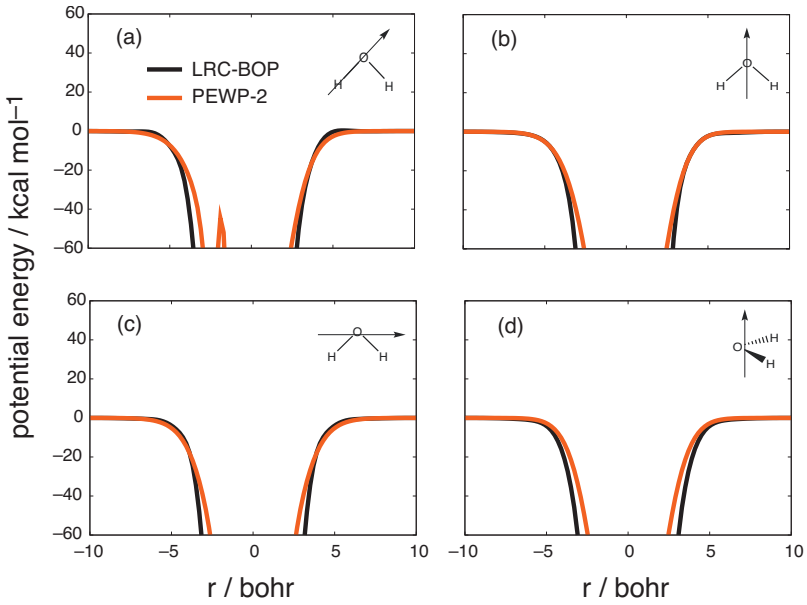

FIG. 2. The LRC-μBOP exchange-correlation potential, obtained from the pseudo-wave function using Eqs. (5) and (6), along with the fit to this potential that is used to construct the PEWP-2 model potential. The origin of the coordinate system is the H_2O center of mass, except in panel (a), where the origin is the oxygen atom.

theory, is reproduced best by the HF pseudo-wave function, but neither pseudo-wave function accurately locates the density maximum along the O–H bond coordinate [see Fig. 3(a)]. We feel that this significant discrepancy reflects an inadequacy in the Phillips–Kleinman procedure,[89] such that a pseudo-potential that is directly fit to the SE pseudo-wave function is likely to afford a one-electron wave function that differs substantially from the SOMO obtained from a many-electron calculation.

We chose to fit our potential to reproduce the position of the density maximum of the LUMO, as computed at the LRC-μBOP level. Figure 3 shows that we are able to fit to the position of this maximum quite well, even if we cannot fit its precise magnitude; in the end, the PEWP-2 density is quite similar to that obtained using the TB potential.[47] The main differences are that our density maximum is slightly closer to the molecular core, and our potential gives an enhanced amount of density just beyond the oxygen atom, in the plane of the molecule [see Fig. 3(c)]. Figure 3 also shows why our previous parametrization, PEWP-1, fails to produce a cavity: there is too much density in the core region. In the one-dimensional slices depicted in Figs. 3(c) and 3(d), for example, the PEWP-1 density achieves nearly its maximum value within the core region. The PEWP-1 repulsive potential is not nearly repulsive enough, and this allows the electron to penetrate easily into the water network, without the need to form a proper cavity, which accounts for the anomalously large diffusion coefficient predicted by this model. This should not be the case with our new parametrization.

The full PEWP-2 potential is compared to PEWP-1 and to the TB potential in Fig. 4, where all three potentials are plotted without polarization. It is clear from Fig. 4 that PEWP-2 contains a steeper and wider repulsive potential than its predecessor; the maximum value of this potential

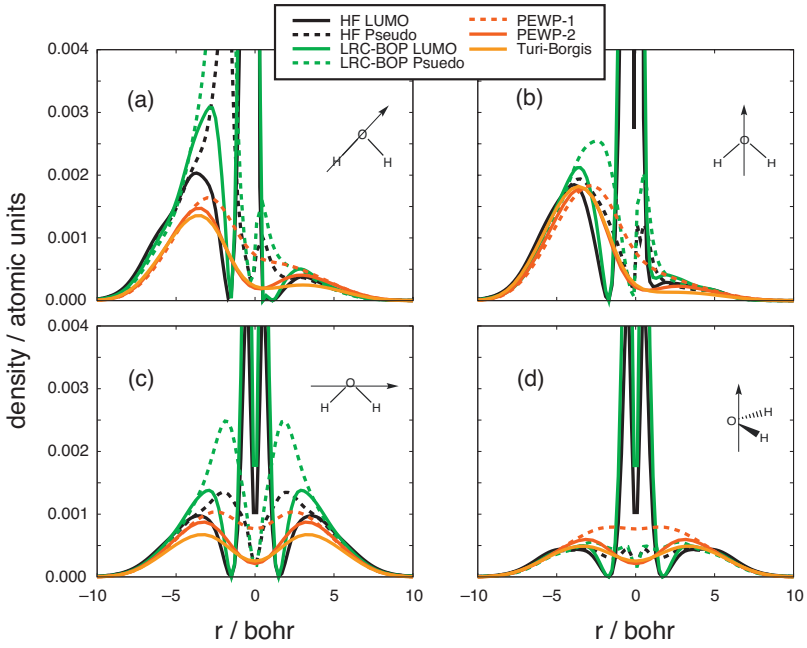

FIG. 3. Comparison of various plots of $|\psi|^2$ for the excess electron obtained using a confining potential (see text for details). The origin of the coordinate system is the H_2O center of mass, except for panel (a), where the origin is the oxygen atom.

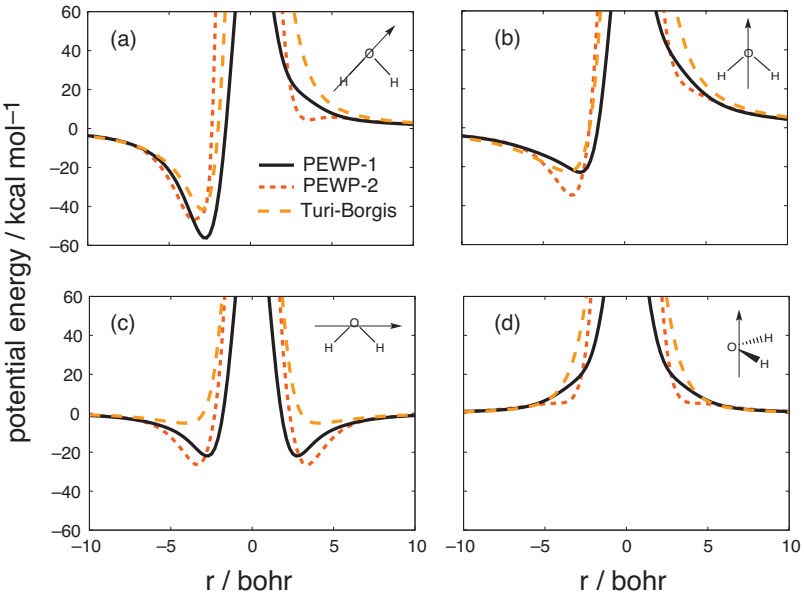

FIG. 4. Comparison of different electron-water potentials, shown without polarization. The origin of the coordinate system is the H_2O center of mass, except for panel (a), where the origin is the oxygen atom.

(not shown in Fig. 4) has increased from ~120 kcal/mol (PEWP-1) to ~550 kcal/mol (PEWP-2). This increase leads to a satisfactory reproduction of the LUMO from LRC-μBOP. The new potential is more attractive along the "dipole" coordinate [Fig. 4(b)], and also along the perpendicular coordinate in the plane of the water molecule [Fig. 4(c)]. These differences largely result from the inclusion of a DFT exchange-correlation potential.

III. COMPUTATIONAL PROCEDURES

Within our model, calculation of energies and wave functions requires simultaneous solution of a grid-based Schrödinger equation,

$$\mathbf{H}\mathbf{c}_I = E_I\mathbf{c}_I, \tag{13}$$

along with linear response equations for the inducible dipoles,

$$\vec{\mu}_i^{\text{ind}} = \alpha_i(\vec{F}_i^{\text{MM}} + \vec{F}_i^{\text{QM}}). \tag{14}$$

Solution of Eq. (13) was accomplished via the Davidson–Liu method,[98] with a convergence threshold of $\|(\hat{H}-E)\psi\| < 10^{-8}E_h$. For $(H_2O)_n^-$ clusters with $n<20$, we use a 60 Å $\times$60 Å $\times$60 Å Cartesian grid with a spacing Δx=1.0 Å, but for larger clusters (where the wave function is more localized), we employ a 40 Å $\times$40 Å $\times$40 Å grid, also with Δx=1.0 Å. These calculations were performed with our home-built code FURRY (version A),[79] which employs a locally modified version of the TINKER MM package[99] to evaluate the AMOEBA water potential and solve for the induced dipoles.

Bulk e_{aq}^- simulations use a grid spacing of $\Delta x \approx 0.93$ Å. This choice is quite conservative, and numerical experiments suggest that the energy is probably converged already with a grid spacing of $\Delta x \approx 1.1$ Å. (The smooth, slowly varying nature of the pseudopotential, combined with the small mass of e^-, enables the use of such a coarse grid.) Simulations were initiated from an equilibrated box of neat liquid water, then allowed to equilibrate for at least 5 ps following introduction of the electron. We propagate the dynamics in the canonical (*NVT*) ensemble using the velocity Verlet algorithm. The water molecules were flexible and a time step of 1.0 fs was used. A single Nosé–Hoover thermostat chain,[100] of length four, was used to conserve temperature.

Electrostatic interactions for bulk e_{aq}^- are treated by standard Ewald summation with a uniform positive background density.[101] For simulations using the TB hydrated-electron model,[47] which includes an *ad hoc* polarization potential of the form given in Eq. (7), the polarization interactions were summed using the minimum-image convention. Nonelectrostatic interactions, including TB polarization, were cut off at one-half of the box length, and were smoothly attenuated starting at 0.95 times that value. (For the 200-molecule unit cell described below, $V_{\text{pol}}<0.04$ kcal/mol at the cutoff distance.)

Regarding Ewald summation, Staib and Borgis[46] point out that because the one-electron wave function interacts with its periodic replicas, the electron-electron interactions should be determined self-consistently, leading to an iterative procedure that is reportedly numerically unstable,[97] and is used infrequently. For the fixed-charge TB model, however, Ewald summation has been shown to increase the bulk VEBE by 0.8 eV relative to the value that is obtained using the minimum-image convention.[52]

From our point of view, solution of the grid-based Schrödinger equation simply requires knowledge of the potential energy at every grid point, and interactions with the image electrons are artifacts of the use of a finite simulation cell, which vanish as the size of the unit cell increases. Therefore, we will run trajectories at several different periodic box sizes in order to extrapolate to the infinite-dilution limit. In our simulations, we evaluate the potential at each grid point as if a $-e$ point charge were located at that grid point, but with induced dipoles that are converged using the actual electric field of the MM molecules and the wave function. Standard Ewald summation is then used to sum all of the electrostatic interactions. We find this procedure to be free of instabilities.

We run trajectories for cubic unit cells containing $N=100$, 200, 300, and 600 water molecules using a water density of 0.997 g/cm^3. (This corresponds to simulation cell lengths $L_{box}=14.4192$, 18.1671, 20.7961, and 26.2015 Å.) For each box size, four independent trajectories were performed, with simulation lengths that varied from 7 ps ($N=600$) to 60 ps ($N=100$), for total simulation times of between 21 and 240 ps.

For simulations involving $N \leq 300$ water molecules, the grid is approximately the same size as the simulation cell, but for ground-state dynamics with $N=600$, we use the same grid as for $N=300$, in order to make the simulation tractable. (Electronic excitation spectra, however, are obtained using grids that fill the entire simulation cell.) Because the electronic energy is not invariant to translation or rotation of the grid, we would like to avoid moving the grid during the simulation, but this is impossible to avoid altogether because the wave function diffuses rapidly through the medium, and would eventually reach the edge of the grid. Energy conservation in the nonpolarizable TB model appears to be relatively insensitive to small translations of the grid, and other researchers have employed a procedure in which the grid is translated at each time step, such that its origin always coincides with the centroid of the wave function.[47,52] In the context of our polarizable model, however, this procedure leads to a catastrophic failure to conserve energy, even though the discontinuities engendered by grid translation change the VEBE by only $\sim 10^{-3}$ eV. Presumably, this enhanced sensitivity arises because the polarizable model uses the grid to discretize not only the potential but also the electric field due to the wave function.

We tested two strategies designed to avoid this problem. The first was to translate the grid to the center of the electron distribution only when $\sim 1\%$ of $|\psi|^2$ resides on the faces of the cubic grid, meaning that the grid is moved as infrequently as possible. A second strategy was to translate the grid by exactly Δx any time that the centroid of ψ is more than Δx away from the origin, so that the new grid exactly coincides with the previous one, albeit shifted by Δx. The first strategy led to good energy conservation until a translation was performed, at which point the system energy dropped discontinuously, by a significant amount ($\sim 0.1\%$). In the smallest simulation cell, translation events occur at least every 10 ps—frequently enough to give us pause. The second strategy conserves energy fairly well in the smallest simulation cell (albeit with a constant drift), but quite well in the largest simulation cell. Using the second strategy, and assuming that the grid is large enough so that the wave function is zero at its edges, the system does not know that the grid has been moved, and energy conservation simply reflects how well the wave function is converged. In the simulations reported below, we employ the second strategy exclusively.

IV. CLUSTER BENCHMARKS

As in our previous work,[79] we assess the accuracy of our one-electron model against MP2 benchmarks for $(H_2O)_n^-$ clusters, $n=2-33$. We will compare PEWP-2 to its predecessor, PEWP-1, and also to the TB model.[47] The latter has been used extensively in recent simulations of both $(H_2O)_n^-$ clusters and also bulk e_{aq}^-.[47–53,63] The TB model employs a nonpolarizable force field for the water molecules,[75] an *ad hoc* electron-water polarization potential [see Eq. (7)], and an electron-water pseudopotential that is fit in order to reproduce the SE pseudo-wave function computed at the HF level. As such, this model provides an appropriate baseline for the performance of the PEWP models, which (in principle) offer a more detailed description of the relevant interactions.

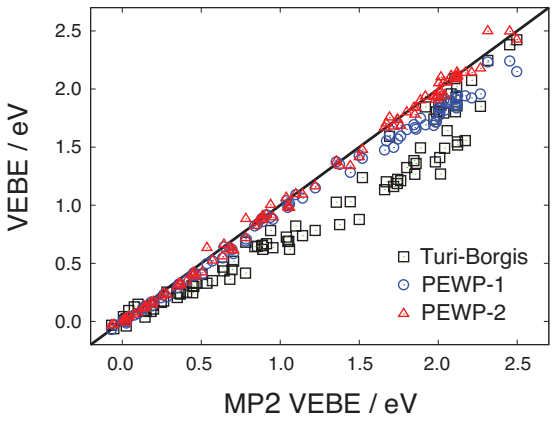

FIG. 5. VEBEs for 95 different $(H_2O)_n^-$ cluster isomers, $n=2-33$, as compared to MP2/6-31(1+,3+)G* benchmarks from Ref. 78.

VEBEs serve as a primary connection between theory and experiment for the hydrated electron, since photoelectron spectra of $(H_2O)_n^-$ have been measured from $n=2$ to $n=200$.[7,8,10,21,28,102] At the same time, accurate prediction of VEBEs is a challenging test of one-electron models, as this requires an accurate description of both the neutral and anionic potential surfaces. In particular, the neutral cluster's potential surface must be described well in regions where the anion is stable, which often correspond to highly distorted hydrogen-bonding networks that lie far above the global minimum on the $(H_2O)_n$ potential surface.[76,77] High-energy configurations are not typically used to parametrize or test interaction potentials that are intended to describe neutral water under ambient conditions.

Benchmark VEBEs for 95 different $(H_2O)_n^-$ cluster isomers, ranging in size from $n=2$ to $n=33$, were obtained from Ref. 78, where they were computed at the MP2/6-31(1+,3+)G* level. We have previously shown that this level of theory is accurate to within $\sim 0.02-0.03$ eV of coupled-cluster results,[60,83,103] and recent quantum Monte Carlo calculations for two different $(H_2O)_6^-$ isomers also agree, within statistical error bars, with both MP2 and coupled-cluster VEBEs.[104] Our VEBE database[78] contains not only gas-phase cluster geometries (optimized using *ab initio* methods), but also clusters that were extracted from bulk simulations using the TB model, and which are therefore more illustrative of bulk e_{aq}^- structure.

Figure 5 compares VEBEs predicted by the various one-electron models to MP2 benchmarks, while Table I summarizes the statistical deviations with respect to MP2 results. Our new model, PEWP-2, is a clear improvement upon both the TB model and also PEWP-1, despite the fact that the

TABLE I. Mean unsigned errors (MUEs) and maximum absolute deviations (MADs) for cluster VEBEs, relative to MP2 benchmarks.

Method	MUE (eV)	MAD (eV)
TB	0.253	−0.746
PEWP-1	0.105	−0.348
PEWP-2	0.041	0.184
LRC-μBOP	0.037	0.224

Coulomb damping parameters in PEWP-1 were fit to reproduce this same set of VEBE benchmarks. Moreover, the PEWP-2 errors do not appear to correlate with cluster size or with the magnitude of the VEBE itself, and all but one of the PEWP-2 VEBEs lie within 0.1 eV of the corresponding MP2 result. The performance of PEWP-2 is similar to that of the LRC−μBOP functional that we used to obtain an exchange-correlation potential.

As in our previous report, we have also evaluated the performance of these models for predicting relative isomer energies in small $(H_2O)_n^-$ clusters, where complete-basis MP2 results are available.[79] The results for our new parametrization are quite good, but do not differ significantly from those obtained for PEWP-1 and discussed in Ref. 79. These data may be found in the supplementary material.[96]

V. BULK SIMULATIONS

The bulk hydrated electron holds an interesting place among aqueous ions, having been deemed, for example, as the "champion structure breaker,"[5] owing to its positive entropy of hydration. As summarized in Sec. I, significant questions remain as to the structure of this species, nevertheless the absorption spectrum,[26,27,70–73] fluorescence spectrum,[13] resonance Raman spectrum,[11–15] entropy of solvation,[5] and diffusion coefficient[6] have all been measured, often under a variety of thermodynamic conditions. Several recent measurements of the bulk VEBE are in reasonable agreement with one another.[30–32] In this section, we examine the PEWP-2 predictions for some of these bulk data.

A. Diffusion coefficient

The diffusion coefficient of e_{aq}^- has been measured over a wide range of temperatures,[6] with a value of $D=0.51$ Å^2/ps obtained at 300 K. The TB model reproduces the temperature dependence of D, and affords a value of 0.6 Å^2/ps at 298 K.[63] For the PEWP-2 model, we have estimated the diffusion coefficient by fitting the long-time slope of the mean displacement, $\langle|\vec{r}(t)-\vec{r}(0)|^2\rangle$.[101] This average converges quite slowly, as there is only a single solute particle, and because our trajectories are fairly short we have only a crude estimate of D for the PEWP-2 model. At 300 K, we obtain $D=0.79\pm0.16$ Å^2/ps, where the uncertainty represents a 95% confidence interval based on the standard deviation over four different trajectories in our smallest box (100 H_2O molecules). Obviously, this is larger than the experimental value; however, the value of D is quite sensitive to temperature,[6,63] and $D=0.79$ Å^2/ps corresponds, experimentally, to $T=317$ K. Reducing the temperature of our simulation by 18 K (to 282 K), we obtain $D=0.65\pm0.18$ Å^2/ps, similar to the TB value and only slightly higher than the experiment, although the uncertainty is considerable. This issue may warrant further investigation in the future, but in any case the agreement with experiment is far more satisfactory than it is for PEWP-1.

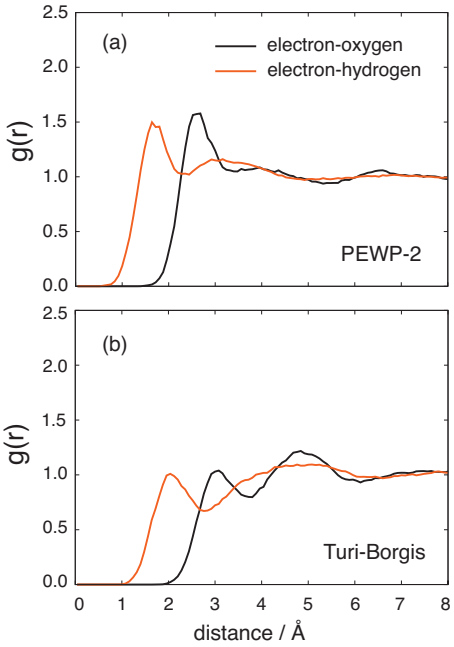

FIG. 6. Radial distribution functions, $g(r)$, for the PEWP-2 and TB models, with respect to the centroid of the electron's wave function.

B. Structure

Radial distribution functions (RDFs) for the oxygen and hydrogen atoms, relative to the centroid of the e_{aq}^- wave function, are shown in Fig. 6 for both the TB and PEWP-2 models. (These RDFs were computed for a unit cell containing 200 water molecules, as we find that structural properties are not strongly affected by the size of the simulation cell.) For both models, integration of the electron-hydrogen RDF up to its first minimum yields a coordination number of four. The cavity size is slightly smaller for our model than for the TB model, with the first hydrogen maximum appearing at 1.7 Å versus 2.0 Å. The average radius of gyration of the electron is also smaller in our model (2.25 Å) than for the TB model (2.45 Å). The first hydrogen (and first oxygen) positions are much more highly correlated with the electron position in our model $[g_{\text{el-H}}(r=1.7\ \text{Å})\sim1.5]$ than in the TB model $[g_{\text{el-H}}(r=2.0\ \text{Å})\sim1.0]$. This is mostly due to the fact that the volume element used to normalize the distributions is smaller in PEWP-2, since the first maximum appears at a smaller distance.

As compared to the TB model, the first oxygen minimum is far shallower and less well-defined for PEWP-2. The RDFs for both models are relatively undercorrelated (in comparison to a more typical anion such as Br^- or I^-), and possess rather broad features. This breadth arises from fluctuations in both the size and shape of the cavity. The initial

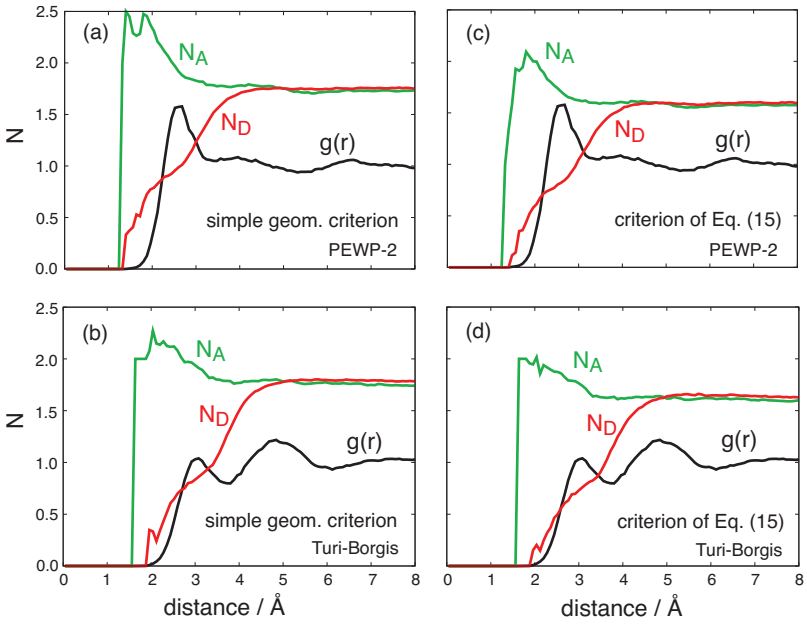

FIG. 7. Average number of hydrogen bonds donated (N_D) and accepted (N_A) per water molecule, as a function of distance from the electron. Also shown is the electron-oxygen RDF, $g(r)$.

rise of the RDFs is noticeably steeper in PEWP-2 than in the TB model, an effect that was also observed with a very early polarizable model for e^-_{aq}.[34]

As mentioned in Sec. I, magnetic resonance experiments in alkaline glasses at $T=77$ K are interpreted in favor of a hexavalent coordination environment for e^-_{aq},[3,4] which is consistent with some theoretical models of e^-_{aq} in liquid water.[40,55,62] An average electron-oxygen distance of ~2.0 Å has also been deduced.[61,62] If this value is characteristic of e^-_{aq} in liquid water under ambient conditions, then our solvation cavity is ~0.3 Å too small, whereas the TB model is about right, although it—like PEWP-2—predicts tetravalent coordination. The notion that the PEWP-2 cavity is ~0.3 Å too small is consistent with a radius of gyration (2.25 Å) that is slightly smaller than the experimental estimate of 2.5 Å that is deduced from a moment analysis of the optical absorption spectrum.[67] It appears that our model's cavity structure is qualitatively correct, although not in quantitative agreement with experiment.

Visual inspection of the PEWP-2 trajectories reveals that the electron is typically coordinated to about four water molecules, but that the arrangement of the O–H bonds is usually far from tetrahedral. Five-coordinate structures also exist, albeit transiently. In contrast, the coordination environment in the TB model is almost always tetrahedral. In PEWP-2, we frequently observe a "bridging" water molecule that donates hydrogen bonds to two different first-shell water molecules, such that the positive end of the bridging molecule's permanent dipole moment is oriented toward the wave function. This behavior is absent in the TB model, most likely owing this model's expanded cavity size. Using PEWP-2, we find that these bridging H_2O molecules can reside very close to the electron, although they are not coordinated to it, and this feature, together with the fleeting pentavalent structures, effectively "washes out" the first minimum in the electron-oxygen RDF.

Tauber and Mathies[15] previously invoked the idea of a disrupted H-bonding network in the vicinity of the electron, in order to rationalize the resonance Raman spectrum of e^-_{aq}, but this aspect of e^-_{aq} solvation does not seem to have been examined with detailed simulations. In order to understand the H-bonding environment nearby the electron, we will examine the average number of hydrogen bonds per water molecule, as a function of the electron-oxygen distance, using two different definitions of what constitutes a hydrogen bond. The first definition, which was used to characterize e^-_{aq} diffusion in a previous study,[63] is that the oxygen-oxygen distance between two H-bonded water molecules is less than 3.5 Å, while at the same time the angle between the covalent O–H bond vector and the O–O vector is less than 30°. We call this the "simple geometric criterion" in the discussion that follows. The second criterion was introduced in Ref. 105, and involves an angle-dependent O–O distance threshold,

$$R(\theta)/\text{Å} = -0.000\,44(\theta/^\circ)^2 + 3.3, \tag{15}$$

for $-50^\circ \le \theta \le 50^\circ$. Here, θ is the aforementioned O–H/O–O angle, and according to this definition, a hydrogen bond exists if the O–O distance is less than or equal to $R(\theta)$. This criterion accounts for the fact that if a particular O–O distance is quite long, then the corresponding angle should be small in order for the two H_2O molecules to be considered H-bonded. Alternatively, if the H-bond angle θ is large, then the O–O distance should be small for H-bonded water molecules. In what follows, we will compare the number of hydrogen bonds predicted by these two definitions; when the simple geometric definition predicts an H-bond but the definition in Eq. (15) does not, we infer that the hydrogen bond in question is a weak one. We will furthermore decompose the average number of H-bonds per H_2O molecule into the number of H-bonds donated (N_D) and the number of H-bonds accepted (N_A).

Figure 7 shows the results of this analysis for both the PEWP-2 and TB models. When the electron-oxygen distance is smaller than the first maximum in the electron-oxygen $g(r)$, we find $N_A \approx 2$ but $N_D < 1$, whereas bulk behavior

($N_A \approx N_D$) is not recovered until $r \approx 5.0$ Å, well into the second solvation shell. These results are independent of which H-bond definition we choose, and also independent of the particular hydrated-electron model (TB or PEWP-2). At the value of r that corresponds to the first maximum in $g(r)$, the simple geometric criterion affords $N_D \approx 1$, exactly what one would expect for coordination involving one O–H bond per H_2O molecule. The criterion of Eq. (15), however, affords a somewhat smaller value of N_D in this region, and in either case N_D increases rapidly as r increases. These observations indicate that water molecules in the first solvation shell are relatively poor H-bond donors. Conversely, first-shell water molecules are excellent H-bond acceptors, especially those nearest the electron; in fact, the simple geometric criterion yields $N_A > 2$ for these innermost water molecules. It is tempting to view this as a polarization effect, since strong interaction with the electron could enhance the H_2O dipole moment, making H-bonds with other water molecules even more favorable, and in fact we do see that PEWP-2 affords slightly larger values of N_A at small r than does the TB model. Even the TB model, however, predicts $N_A > 2$ at small r. If we substitute the H-bond definition in Eq. (15), then the maximum value of N_A is reduced to ≈2, suggesting that any H-bonds accepted in excess of two per H_2O molecule are fairly weak.

In our view, the weak H-bond-donating capability of first-shell water molecules arises from the diffuse nature of the ion, which provides relatively little restoring force for water librations, as compared to a hydrated halide ion, for example. Thus, we expect H_2O molecules in the first shell to undergo fairly large-amplitude motion, as compared to bulk H_2O, making for poor H-bond donation. This does not necessarily mean that the same first-shell H_2O molecule cannot *accept* hydrogen bonds, however. In fact, since the electron orients water molecules even in the second solvation shell, this has the effect of enhancing the number accepted H-bonds in the first shell.

C. Librational dynamics

In Sec. V B, we hypothesized that water molecules nearby the electron are subject to enhanced librational motions. To substantiate this claim, we next examine the librational dynamics of individual H_2O molecules as a function of their distance from the centroid of the e^-_{aq} wave function. In order to separate librational and vibrational motions as much as possible, we first determine the Eckart frame[106] for each water molecule. We then compute an autocorrelation function,

$$C(t) = \left\langle \sum_i \vec{\Omega}_i(0) \cdot \vec{\Omega}_i(t) \right\rangle, \tag{16}$$

where $\vec{\Omega}_i$ represents a unit vector along one of the Eckart axes, for the ith water molecule, and the summation runs over a restricted set of water molecules, as detailed below. Angle brackets in Eq. (16) indicate an ensemble average. A similar approach has previously been used to characterize librational dynamics in neat liquid water.[107]

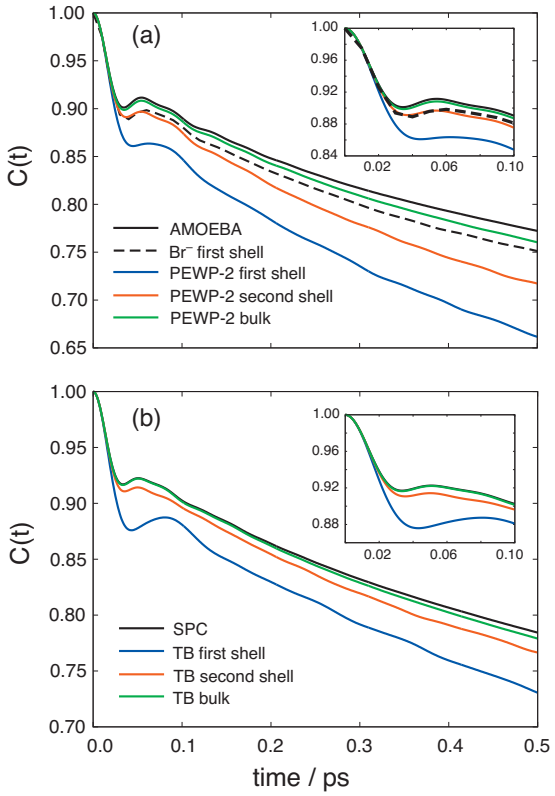

FIG. 8. Early-time behavior of the orientational time correlation function $C(t)$ [Eq. (16)] for neat liquid water and for e^-_{aq} at various distances from the electron (see text for details). In (a), the neat liquid is described by the AMOEBA force field and e^-_{aq} by the PEWP-2 model; in (b), the SPC model is used for liquid water and the TB model for e^-_{aq}. Panel (a) also shows results for aqueous Br^- described using the AMOEBA force field. The correlation function $C(t)$ is computed for a periodic simulation cell containing 200 water molecules.

In order to analyze the dynamics near the electron, we compute the average in Eq. (16) using only those water molecules that, at $t=0$, lie within a specified distance of the centroid of the electron's wave function. Because this distance changes as a function of time, our analysis is limited to the short-time behavior of $C(t)$. We investigate the dynamics in three regions: from $r=0$ up to the first oxygen minimum ($r=3.2$ Å for PEWP-2 and $r=3.8$ Å for TB); from the first oxygen minimum out to $r=5.0$ Å; and finally, $r>5.0$ Å. We refer to these regions as the first solvation shell, second solvation shell, and bulk water, respectively.

Figure 8 shows $C(t)$ evaluated for a unit vector along the C_2 Eckart axis. (Qualitatively similar results are obtained for all three Eckart axes.) For neat liquid water, $C(t)$ exhibits an ultrafast inertial response at short times followed by a small recoil prior to the onset of a long-time exponential decay.[107] We are interested in the dynamics prior to the exponential decay.

For neat liquid water, $C(t)$ decays from unity to a value of ~0.9 over the first 34 fs, corresponding to a rotation angle of about 25°. Between 34 and 54 fs, the water molecule recoils slightly, as evidenced by a "hump" in $C(t)$ centered around 54 fs. By comparison, the initial Gaussian decay is more pronounced for water molecules in the first shell of e^-_{aq}, and furthermore the average angle prior to recoil increases by 5° and the time period prior to recoil increases by 10 fs,

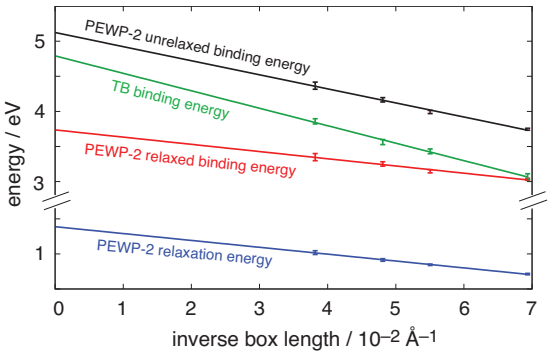

FIG. 9. Extrapolation of the VEBE as a function of inverse simulation cell length, $1/L_{box}$. Error bars represent a 95% confidence interval at each box size.

relative to neat liquid water. For the PEWP-2 model, the recoil maximum in $C(t)$ is almost completely absent for first-shell waters, while the TB model shows only a very slow recoil, with a maximum at 80 fs. This is much slower than the 51 fs that is observed for the underlying SPC water model. In contrast, the librational dynamics for first-shell water molecules in aqueous Br^- (as described by the AMOEBA force field) are much faster compared to those in e^-_{aq}, and closely resemble the dynamics of water molecules in the *second* solvation shell around e^-_{aq}.

We interpret the enhanced Gaussian decay and attenuated recoil as evidence of enhanced librations due to smaller restoring forces for hindered rotation near the electron. That is, the inertial decay of $C(t)$, corresponding to quasifree rotation of H_2O, lasts slightly ($\sim$10 fs) longer nearby the electron. In addition, the recoil following this event is attenuated. This indicates that librational motion is amplified, and that the restoring forces that lead to recoil are damped. Surprisingly, second-shell water molecules also show enhanced librational dynamics, albeit to a much lesser extent than is observed in the first solvation shell. At distances greater than 5.0 Å, the librational dynamics are essentially identical to those in bulk water. These data support our earlier contention that hydrogen bonding is disrupted by enhanced librational dynamics in the first two solvation shells, with bulk-like behavior recovered in the third solvation shell.

D. Vertical electron binding energy

To determine the VEBE of bulk e^-_{aq}, we calculate the average VEBE at each simulation cell size, and then extrapolate to the infinite-dilution ($L_{box}\rightarrow\infty$) limit. For a charged system, the long-range interactions in a Ewald sum converge slowly, and one expects that the VEBE will converge as $1/L_{box}$,[108,109] which is precisely what we observe in practice. Extrapolations to $L_{box}=\infty$ are depicted in Fig. 9, where error bars are determined by propagating the statistical error in the mean for each simulated VEBE, and are reported at the 95% confidence level.

For the TB model, the VEBE is (up to a sign) simply the ground-state electronic energy, and extrapolates to a value of 4.79 ± 0.09 eV at infinite dilution. This is considerably larger than all previous reports of this quantity using the TB model; these include a value of 3.12 eV calculated using the minimum-image convention,[47] a value of 3.9 eV determined using Ewald summation (with an unspecified simulation cell size),[53] and a value of 4.4 eV determined by extrapolating cluster VEBEs.[53] That our Ewald-summed value is so much larger than the one reported in Ref. 53 is not altogether surprising, given the sensitivity of the VEBE to L_{box} that is seen in Fig. 9, but it is curious that our infinite-dilution value is 0.3–0.4 eV larger than that reported based on cluster extrapolation.

The MM inducible dipoles in our model represent electronic degrees of freedom, albeit coarse-grained ones, and these ought to remain in equilibrium with the electron, relaxing on the same time scale as electronic excitation or electron detachment. Figure 9 shows three separate extrapolations for the PEWP-2 model: a "relaxed" binding energy, an "unrelaxed" binding energy, and the difference between the two, which we call the relaxation energy. The latter is the energy associated with electronic reorganization of the solvent, i.e., changes in the MM inducible dipoles upon electron detachment.

The slope and intercept of the unrelaxed binding energy extrapolation are similar to those obtained for the TB model, where no relaxation is possible, which makes sense because the dielectric constant of the two systems should be quite similar. However, the relaxed binding energy in our model extrapolates to a much smaller value, 3.70 ± 0.071 eV. This value lies between the value of 4.0 eV that is obtained by extrapolating VEBEs for $(H_2O)^-_n$ clusters collected in an ion trap ($T\approx10$ K),[28] and the value of 3.4 eV that is obtained by extrapolating VEBEs for warmer clusters.[66] Our predicted VEBE is also larger than the value of 3.3 eV obtained in two recent liquid microjet experiments,[30,31] but is within error bars of a third liquid jet measurement, 3.6 ± 0.1 eV.[32] Considering that the ion trap experiments likely probe ice-like clusters, experimental estimates for the liquid-phase VEBE lie in the range of 3.3–3.6 eV; our model's prediction is far closer to these values than is the TB value, when the latter is calculated in a rigorous way.

The relaxation energy extrapolates to a surprisingly large value of 1.37 ± 0.04 eV, which reveals an important fact about nonpolarizable solvated-electron models. Specifically, it explains how the TB model can be systematically underbinding in small clusters (Fig. 5), yet overbinding in the bulk limit (Fig. 9). This does not necessarily imply that the nonpolarizable models are inherently flawed, since this relaxation energy does not affect the ground-state forces, and ground-state structure and dynamics may therefore be largely insensitive to the lack of polarization. At the same time, it is clear that some correction needs to be applied to binding energies calculated using nonpolarizable models, especially in the bulk limit. We expect this to be the case in any polarizable medium, not just water.

Recently, Madarász *et al.*[53] extrapolated $(H_2O)^-_n$ cluster binding energies for cavity states, calculated using the nonpolarizable TB model, and obtained a value of $\sim$4.4 eV. These authors then compare to a Born-like dielectric continuum model developed by Makov and Nitzan,[110] obtaining VEBEs that are surprisingly consistent with those obtained from atomistic simulations. Madarász *et al.* employ the

TABLE II. Input parameters and results from application of the dielectric continuum model developed in Ref. 110.

	One-electron model	
Property	TB	PEWP-2
$\langle r_g \rangle$/Å	2.45	2.25
$\langle \hat{T} \rangle$/eV	1.6	1.7
VEBE (ϵ_∞=1.0)/eV	4.2	4.6
VEBE (ϵ_∞=1.8)/eV	2.9	3.2
Relaxation energy/eV	1.3	1.4

Makov–Nitzan model with an optical (infinite-frequency) dielectric constant $\epsilon_\infty=1$, consistent with a nonpolarizable model. Here, we calculate the relaxation energy predicted by this same continuum model, using water's actual optical dielectric constant, $\epsilon_\infty=1.8$.[110] Instead of using this model to predict VEBEs of spherical clusters, we will investigate a situation where the electron is embedded in an infinite dielectric. We compare VEBEs obtained for $\epsilon_\infty=1.0$ versus $\epsilon_\infty=1.8$, and take the difference to be a continuum approximation for the relaxation energy.

The parameters required for the continuum model are the electronic kinetic energy, a cavity radius for the ion (which we take to be the electron's radius of gyration, r_g), and the static and optical dielectric constants.[110] We use $\langle \hat{T} \rangle$ and $\langle r_g \rangle$ determined from simulation and a static dielectric constant of $\epsilon=78$. The results (Table II) are a relaxation energy of 1.3 eV for the TB model and 1.4 eV for PEWP-2, in excellent agreement with the value extrapolated from simulations with explicit many-body polarization. If the extrapolated TB binding energy from Fig. 9 is reduced by 1.3 eV, we obtain a bulk VEBE of 3.5 eV. This modified value is in good agreement with the value of 3.7 eV that is extrapolated for PEWP-2 (see Fig. 9), especially considering that cluster benchmarks indicate that the TB model is underbinding, relative to PEWP-2, by ~0.25 eV.

E. Optical absorption spectrum

Whereas VEBEs are important experimental handles for $(H_2O)_n^-$ clusters, optical absorption spectroscopy is the primary means of detecting and characterizing e_{aq}^- in bulk liquids. The absorption spectrum of e_{aq}^- in ambient liquid water is broad and featureless, peaked at 1.72 eV with a Gaussian rise on the low-energy side of the spectrum and a Lorentzian decay on the blue edge (see Fig. 10).[66] Of the one-electron models that have been brought to bear on this problem, the TB model affords the best estimate of the absorption maximum, with a prediction of 1.92 eV,[47] whereas other one-electron models put this maximum at still higher excitation energies. Turi and Borgis[47] claim that a self-consistent treatment of solvent electronic polarization in the excited state should bring the absorption maximum into good agreement with experiment, an assertion that will be tested here. More importantly, the Lorentzian tail in the spectrum has not been reproduced by any computational means,[54] prior to a recent preliminary account of our PEWP-2 results,[64] which are discussed in more detail here.

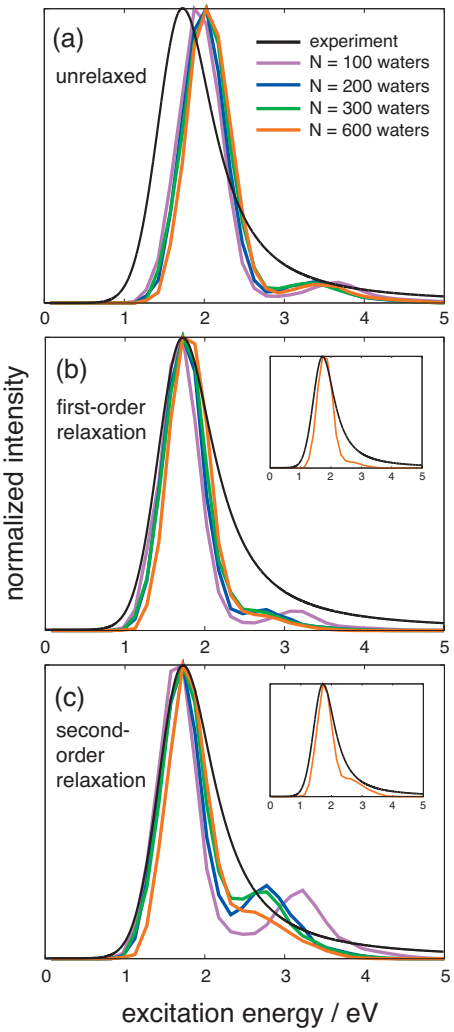

FIG. 10. Bulk absorption spectra for e_{aq}^-, calculated using various box sizes and various treatments of the solvent's electronic relaxation energy, including (a) neglect of the perturbation $\hat{W}_n$, (b) first-order correction for $\hat{W}_n$, and (c) second-order correction for $\hat{W}_n$. Insets in (b) and (c) compare the experimental spectrum (obtained from line shape parameters in Ref. 66) to results computed with our largest simulation cell.

We simulate the absorption spectrum by computing oscillator strengths

$$f_{0\to n}=\frac{2m_e}{3\hbar^2}(E_n-E_0)\sum_{\kappa\in\{x,y,z\}}|\langle\psi_0|\hat{\kappa}|\psi_n\rangle|^2 \tag{17}$$

between the ground state and the lowest 29 excited states ($n\leq 29$), at each of ~1000 snapshots sampled from ground-state molecular dynamics. The absorption spectrum is obtained as a histogram of excitation energies, weighted by the corresponding oscillator strengths. Within our polarizable model, however, the treatment of the excited-state wave functions is not entirely straightforward, as we next discuss.

Because the inducible H_2O dipoles represent electronic degrees of freedom, it is physically reasonable that they should remain in equilibrium with the wave function upon electronic excitation. In principle, one could imagine a self-consistent procedure to converge the dipoles and wave function for each excited state, but we have found that such procedures have serious convergence problems owing to the fact

TABLE III. Parameters E_{max} and σ_G, both in eV, for fitting the low-energy Gaussian portion of the absorption spectrum [see Eq. (19)]. The quantities N and L_{box} specify the number of water molecules and the length of the simulation cell, respectively.

		Unrelaxed		First-order		Second-order	
N	L_{box} (Å)	E_{max}	σ_G	E_{max}	σ_G	E_{max}	σ_G
100	14.4	1.94	0.27	1.69	0.24	1.65	0.24
200	18.2	1.99	0.26	1.74	0.25	1.70	0.26
300	20.8	2.02	0.29	1.75	0.26	1.73	0.27
600	26.2	2.04	0.25	1.78	0.23	1.77	0.24
Expt.[a]						1.72	0.30

[a]Experimental line shape parameters from Ref. 66.

that the polarization energy is quite large in comparison to the small energy gaps between excited states. As such, states may "switch" during the Davidson iterations. As an alternative, we employ a state-specific perturbation theory in order to calculate relaxed excited-state wave functions and electronic energies. To obtain the perturbation, we first calculate the ground-state wave function $|\psi_0\rangle$ and an excited-state wave function $|\psi_n\rangle$ using dipoles $\{\vec{\mu}_i^{(0)}\}$ that are converged to $|\psi_0\rangle$. We then obtain new dipoles $\{\vec{\mu}_i^{(n)}\}$ that are converged to $|\psi_n\rangle$, without relaxing the latter. The quantity

$$\hat{W}_n = \hat{H}[\{\vec{\mu}_i^{(n)}\}] - \hat{H}[\{\vec{\mu}_i^{(0)}\}] \tag{18}$$

is taken to be the perturbation for state $|\psi_n\rangle$.

One difficulty with the aforementioned procedure is that of orthogonality. Each relaxed excited state is an (approximate) eigenvector of a different Hamiltonian, and therefore these states need not be mutually orthogonal. As such, one might anticipate spurious intensity enhancements due to nonorthogonality. Furthermore, if the quantum states are not orthogonal then the transition dipole matrix elements are not invariant to translation of the coordinate origin. In order to avoid the latter problem, we do not allow the excited states to mix with the ground state in the perturbative expansion of the wave function. This at least ensures that $\langle\psi_0|\psi_n\rangle=0$, even if the excited states are not mutually orthogonal.

Figure 10 compares the experimental absorption spectrum to spectra computed using various corrections for the perturbation $\hat{W}_n$. Unrelaxed spectra [Fig. 10(a)] correspond to a complete neglect of $\hat{W}_n$, i.e., only ground-state dipoles are involved in the calculation. The relaxed spectra [Figs. 10(b) and 10(c)] include corrections for $\hat{W}_n$ based on either first- or second-order perturbation theory. In addition, we also compare spectra computed using different periodic cells. (Since many of the higher-lying states are quite diffuse, for the excited-state calculations we use a grid that fills the entire simulation cell.)

The unrelaxed spectra [Fig. 10(a)] are insensitive to the size of the simulation cell, and are quite similar to the spectrum obtained using the nonpolarizable TB model.[47,64] The absorption maximum in these spectra is slightly blue-shifted relative to experiment; upon fitting the low-energy portion of the spectrum to a Gaussian,

$$I(E) = A\ \exp[-(E-E_{max})^2/2\sigma_G^2], \tag{19}$$

we obtain $E_{max}\approx 2.0$ eV and $\sigma_G\approx 0.25$ eV. (Gaussian fitting parameters are listed in Table III, where they are compared to experimental line shape parameters.) While E_{max} is 0.3 eV higher than the experiment, the Gaussian width of the unrelaxed spectrum is reasonably accurate.

A first-order treatment of $\hat{W}_n$ dramatically red-shifts the spectrum [Fig. 10(b)], bringing the absorption maximum into excellent agreement with experiment, while changing σ_G by only 0.02 eV. Thus, the Gaussian part of the experimental spectrum is reproduced quantitatively using first-order relaxation, and essentially no further change in the Gaussian feature is observed at second order. The contention of Turi and Borgis,[47] that excited-state electronic polarization would red-shift the spectrum by 0.2–0.3 eV, appears to be correct. What was not anticipated is the effect of polarization on the blue tail.

Figure 11 decomposes the computed absorption spectra, for the largest simulation cell, into contributions arising from various categories of excited states. Consistent with the results of previous simulations,[40,41,47,54] we find that most of the absorption intensity is carried by three p-type states that give rise to a broad Gaussian profile. This part of the spectrum is converged even in the smallest simulation cell, and the red edge (up to the absorption maximum) is in quantitative agreement with experiment. At higher excitation energies, however, the unrelaxed spectrum exhibits a gap, with very little spectral intensity, rather than the smooth tail that is observed experimentally. Above this gap is a weak tail comprised of excitations to unbound states, i.e., a photoelectron spectrum. (We categorize states as being bound or unbound based on whether or not the excitation energy exceeds the VEBE. This definition does not preclude the possibility that some of these vertically bound excitations are *adiabatically* unbound.)

First-order relaxation red-shifts the higher-lying states to a greater extent than the $1p$ states, resulting in a smoother decay of the spectrum at high energy, without so much of the aforementioned gap in intensity. The distribution of oscillator strengths changes only slightly, however, since first-order relaxation can alter $f_{0\to n}$ only through the excitation energy, E_n-E_0 [see Eq. (17)]. Whereas the first 29 excited states account for 95% of the total oscillator strength, this figure drops to 80% upon first-order relaxation. This decrease in

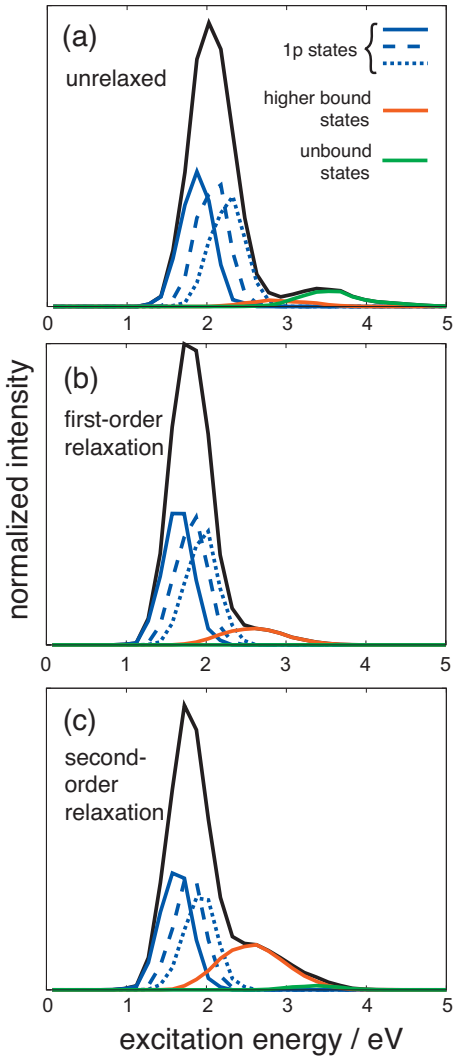

FIG. 11. Computed absorption spectra for e^-_{aq}, decomposed into various categories of excited states, using our largest simulation cell (N=600 water molecules).

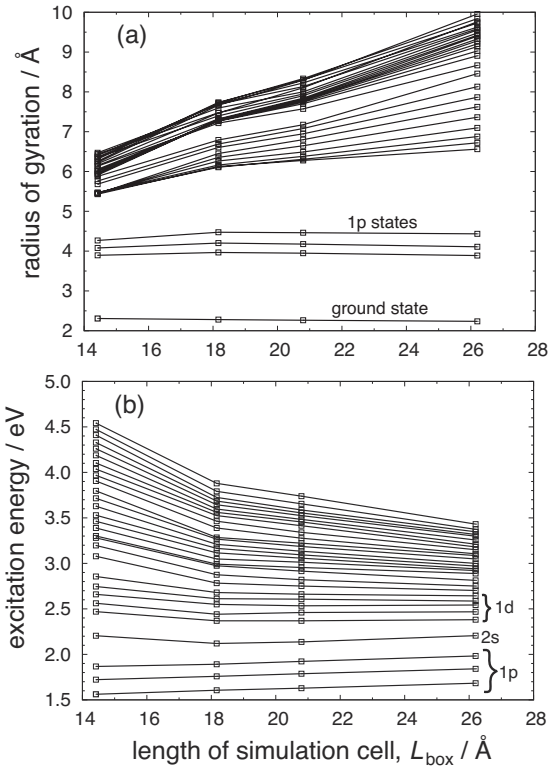

FIG. 12. Average values of (a) the radius of gyration and (b) the excitation energy, as a function of L_{box}, for each of the lowest 29 electronic states of e^-_{aq}.

oscillator strength is understandable, given that first-order relaxation does not alter the transition dipoles, therefore $f_{0\to n}$ must decrease, according to Eq. (17).

At second order, one obtains a correction to the wave function and therefore the transition dipoles, which allows the unrelaxed excited states to mix with the $1p$ states and thereby acquire oscillator strength.[111] The result [Fig. 11(c)] is a significant intensity enhancement in the blue tail, relative even to the first-order result. At the same time, the $1p$ states are still clearly responsible for the Gaussian feature in the absorption spectrum. The feature labeled "unbound states" has almost disappeared in the relaxed spectra shown in Fig. 11, because relaxation leads to a considerable increase in the number of bound states; of the 29 states that comprise the spectra in Fig. 11, an average of 25.6 are bound at second order (collectively accounting for 90% of the total oscillator strength), whereas only 6.9 excited states are bound, on average, when relaxation is neglected. We expect that the "unbound" feature would return if we calculated additional excited states.

Beyond the $1p$ states, the excited states are quite diffuse and are not adequately represented in small simulation cells. (Snapshots of the PEWP-2 excited-state wave functions can be found in Ref. 64.) In small unit cells, the second-order relaxation correction (and accompanying intensity borrowing by the higher-lying states) leads to a hump on the blue edge of the spectrum, but this feature shifts to lower energy as L_{box} increases, ultimately producing a smooth tail in our largest simulation cell.

Figure 12 plots the average excitation energy and radius of gyration, r_g, for each electronic state as a function of L_{box}. For the ground state and the $1p$ states, r_g is essentially independent of L_{box}, but for the higher-lying excited states r_g increases steadily as the box (and the grid) are extended. The highest-energy states that we calculate are probably not converged with respect to the size of the unit cell, and a further increase in L_{box} would likely result in a further red-shift of these states that would improve the agreement with experiment around 2.5 eV. Nevertheless, it is clear that the qualitative effect of the solvent's electronic relaxation is to create "polarization-bound" excited states that give rise to a continuous blue tail, without the gap in oscillator strength that is observed in both the unrelaxed spectrum and in the spectra calculated using nonpolarizable models.

These observations lead us to the following interpretation of the bulk e^-_{aq} absorption spectrum. The Gaussian feature on the low-energy side of the spectrum arises from three $1s\to 1p$ excitations, as many previous studies have also concluded.[40,41,47,54,58,62,64] The blue tail, however, arises from excitations into diffuse quasicontinuum states that are bound (in a vertical sense) entirely by the instantaneous polarization

of the solvent upon excitation of the unpaired electron. These states acquire intensity via solvent-facilitated intensity borrowing from the $1p$ states, which are the only bright states in a spherical cavity model.[111]

Although the high-energy edge of our computed spectrum is not in quantitative agreement with experiment, it is vastly improved relative to that predicted using nonpolarizable models. We note that our calculations do not include any sort of lifetime broadening, which could be important given the high spectral density beyond the $1p$ manifold [see Fig. 12(b)], and might be the origin of the Lorentzian line shape that is observed experimentally. Another source of error in the high-energy line shape is that our model includes the solvent's contribution to the oscillator strengths only indirectly, via the response of the electron's wave function to changes in the MM dipole parameters. In a fully QM treatment, the H_2O dipole moments would contribute to the dipole moment operator in Eq. (17).

Shkrob *et al.*[62] reported mixed quantum mechanics/molecular mechanics (QM/MM) calculations of the e^-_{aq} absorption spectrum, at the QM level of singles configuration interaction, but these calculations did not result in a blue tail. These authors acknowledge that the higher-lying states are quite diffuse, and it is unclear whether the QM region in these calculations is sufficient to describe these states. The blue tail is also absent in the Kohn–Sham density of states obtained from a Car–Parrinello simulation of e^-_{aq}.[58] However, we have recently reported time-dependent DFT simulations of the e^-_{aq} absorption spectrum, using a QM/MM formalism in conjunction with the LRC-μBOP density functional, and these calculations *do* result in a substantial blue tail.[64] We find that a sizable QM region (somewhat larger than that used by Shkrob *et al.*[62]) is required in order to obtain this tail, which we interpret as additional evidence that solvent polarization does indeed facilitate intensity borrowing by higher-lying excited states.

F. Polarized transient hole-burning

A long-standing discrepancy between experiment and one-electron simulations of e^-_{aq} concerns whether the Gaussian part of the absorption spectrum is primarily homogeneously or inhomogeneously broadened.[112] Most previous simulations suggest inhomogeneous broadening that should be detectable via a polarized transient hole-burning (PTHB) experiment,[44,45] wherein a polarized pump laser is used to excite a subpopulation of the $1s \rightarrow 1p$ band, leading to a bleach in the signal arising from a second, polarized probe laser.[112] Although the first PTHB experiments appeared to confirm this prediction,[113] subsequent experiments failed to detect the anisotropic bleaching dynamics that would indicate inhomogeneous broadening.[112,114,115]

Observation of polarization dependence in the bleaching dynamics requires three properties. First, the three $1p$ subpopulations must be sufficiently well-separated so that the pump pulse can excite primarily a single subpopulation; second, the three $1s \rightarrow 1p$ transition dipole moments must be orthogonal, or very nearly so; and third, the reorientation of these transition dipoles, due to fluctuations in the asymmetry of the cavity, must be slow enough to be detectable via femtosecond spectroscopy. According to the absorption spectrum calculated using our model (Fig. 11), electronic relaxation of the solvent causes the three $1s \rightarrow 1p$ subbands to overlap more strongly than they do in the absence of relaxation, such that to pump just a single $1s \rightarrow 1p$ transition probably requires excitation at either the red edge or the blue edge of the Gaussian feature. However, our results suggest that the $1s \rightarrow 1p$ excitations near the blue edge are strongly overlapped by quasicontinuum transitions that, as Schwartz and coworkers point out,[112] are unlikely to have sufficient asymmetry in their transition dipoles (if indeed they are polarized at all) to observe polarization-dependent anisotropy. According to our model, then, the only way in which one might expect to observe PTHB dynamics is by exciting on the extreme red edge of the absorption spectrum. Such an experiment has been reported,[112] but no significant polarization dependence was observed in the bleaching dynamics.

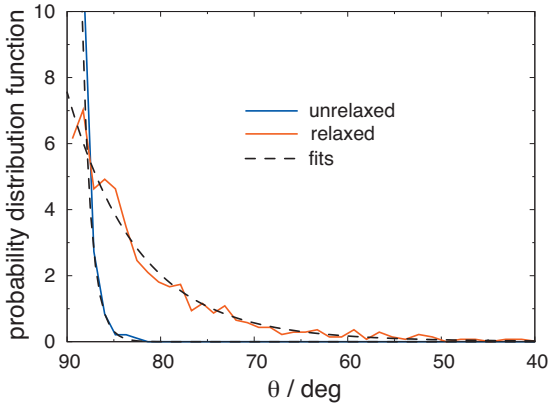

FIG. 13. Probability distribution functions for the angle between the transition dipole moments of the three $1s \rightarrow 1p$ excitations, along with fits to single-exponential decay curves.

Assuming that our model describes the excited states correctly, and assuming that selective excitation of the lowest-lying $1p$ state is indeed feasible, our model suggests that one might still fail to observe PTHB dynamics. To see why, we plot in Fig. 13 the probability distribution function for θ, the angle between the $1s \rightarrow 1p$ transition dipole moment vectors. In the absence of electronic relaxation of the solvent, these three vectors are nearly orthogonal, with $\theta > 85°$ in nearly every case. Allowing for second-order relaxation, however, we obtain a much broader distribution in θ, with some amplitude all the way out to at least $\theta = 60°$. Thus, the relaxed transition moments are not strictly perpendicular, even though the excited-state wave functions are clearly p-like. Thus, even if it proves feasible to separate the three $1s \rightarrow 1p$ excitations on an energetic basis, one would still have difficulty distinguishing the populations based upon their orientation. Furthermore, Shkrob[116] calculated an autocorrelation function for rotation of the $1s \rightarrow 1p$ transition dipole moments, and found that this correlation function decays on a time scale of $\sim$100 fs. Together, these observations indicate that the PEWP-2 model of e^-_{aq} is consistent with the lack of observed PTHB dynamics.

It is worth noting that Larsen *et al.*[65] used similar argu-

ments to explain the lack of PTHB dynamics in their e^-_{aq} model, which does not form a cavity. Indeed, because earlier, cavity-forming models *did* predict observable PTHB dynamics, this argument was used as evidence in support of the newer model, with its much more diffuse electron.[65] At the very least, the results in this section demonstrate that lack of PTHB dynamics need not be inconsistent with a cavity-bound electron.

VI. SUMMARY AND CONCLUSIONS

We have described a reparametrization of a polarizable electron-water interaction potential, PEWP-2, leading to a new hydrated-electron model in which many-body electron-water polarization is included in a self-consistent way. Unlike our previous model (PEWP-1),[79] which afforded promising results for $(H_2O)^-_n$ clusters but failed to localize the electron in the condensed phase, the new parametrization performs at least as well for clusters (as judged by comparison to *ab initio* benchmarks), but also qualitatively reproduces various experimental data for e^-_{aq} in bulk water. As Shkrob *et al.*[61,62] and others[29,59] have argued, quantitative reproduction of structural features and experimental parameters may require many-electron quantum mechanics. Nevertheless, the PEWP-2 model affords a VEBE and an optical absorption spectrum that are in far better agreement with experiment than are previous one-electron models, while structural and dynamical features, such as the radius of gyration and diffusion coefficient, are at least qualitatively correct.

For e^-_{aq} in bulk water, we have demonstrated that H_2O molecules in the first solvation shell are poor H-bond donors but good H-bond acceptors, a result that we can also reproduce using a nonpolarizable model. This disruption in the H-bonding environment is caused by enhanced librational motions of water molecules nearby the solvated electron, and may be related to the electron's anomalously large entropy of hydration.

By extrapolating the bulk VEBE to the infinite-dilution limit, we predict a bulk binding energy of 3.7 eV, a value that is slightly smaller than the most recent extrapolation of cluster photoelectron data,[28] but is 0.3 eV higher than previous extrapolations.[66] Our value is 0.4 eV higher than two recent direct measurements of the VEBE using liquid microjets,[30,31] but is in good agreement with a third liquid microjet experiment.[32] The discrepancy between these various values underscores the need for models such as the one constructed here, which can reproduce both qualitative characteristics of bulk e^-_{aq}, but are also quantitatively accurate for cluster VEBEs.

The importance of self-consistent, many-body electron-water polarization has been demonstrated in two very important ways. First, we have shown that the electronic reorganization energy that accompanies electron detachment is quite large ($\approx$ 1.4 eV) in the bulk limit. This observation indicates that nonpolarizable models can dramatically overestimate VEBEs in large systems, while simultaneously underestimating VEBEs in the small $(H_2O)^-_n$ clusters that are often used as benchmarks. A second key effect of self-consistent polarization is a qualitative change in the line shape of the optical absorption spectrum for e^-_{aq}, bringing the predicted spectrum into much closer agreement with experiment than has been seen in any previous one-electron model. Inclusion of electronic relaxation of the solvent upon excitation of the one-electron wave function has the effect of red-shifting the absorption maximum by 0.3 eV, placing it in remarkable agreement with experiment. Furthermore, relaxation greatly increases the number of (vertically) bound electronic states, leading to a smooth tail on the blue edge of the absorption spectrum. This blue tail has proven elusive in previous simulations,[54] but in our model it arises naturally due to solvent-facilitated intensity borrowing by quasicontinuum excited states.

It is our hope that this potential will ultimately be useful in interpreting photoelectron experiments for $(H_2O)^-_n$ clusters, and for studying the ground- and excited-state dynamics of the solvated electron in bulk water. Work along these lines is in progress.

ACKNOWLEDGMENTS

The authors thank J. V. Coe and S. E. Bradforth for numerous discussions. This work was supported by a National Science Foundation CAREER award (Grant No. CHE-0748448), and calculations were performed at the Ohio Supercomputer Center under Project No. PAS-0291. J.M.H. gratefully acknowledges a fellowship from the Alfred P. Sloan Foundation.

[1] E. J. Hart and J. W. Boag, J. Am. Chem. Soc. **84**, 4090 (1962).
[2] J. W. Boag and E. J. Hart, Nature (London) **197**, 45 (1963).
[3] L. Kevan, J. Phys. Chem. **85**, 1628 (1981).
[4] L. Kevan, Acc. Chem. Res. **14**, 138 (1981).
[5] P. Han and D. M. Bartels, J. Phys. Chem. **94**, 7294 (1990).
[6] K. H. Schmidt, P. Han, and D. M. Bartels, J. Phys. Chem. **99**, 10530 (1995).
[7] J. V. Coe, G. H. Lee, J. G. Eaton, S. T. Arnold, H. W. Sarkas, K. H. Bowen, C. Ludewigt, H. Haberland, and D. R. Worsnop, J. Chem. Phys. **92**, 3980 (1990).
[8] G. H. Lee, S. T. Arnold, H. W. Sarkas, K. H. Bowen, C. Ludewigt, and H. Haberland, Z. Phys. D: At., Mol. Clusters **20**, 9 (1991).
[9] P. Ayotte and M. A. Johnson, J. Chem. Phys. **106**, 811 (1997).
[10] J. Kim, I. Becker, O. Cheshnovsky, and M. A. Johnson, Chem. Phys. Lett. **297**, 90 (1998).
[11] M. Mizuno and T. Tahara, J. Phys. Chem. A **105**, 8823 (2001).
[12] M. Mizuno and T. Tahara, J. Phys. Chem. A **107**, 2411 (2003).
[13] M. J. Tauber and R. A. Mathies, J. Phys. Chem. A **105**, 10952 (2001).
[14] M. J. Tauber and R. A. Mathies, Chem. Phys. Lett. **354**, 518 (2002).
[15] M. J. Tauber and R. A. Mathies, J. Am. Chem. Soc. **125**, 1394 (2003).
[16] N. I. Hammer, J. W. Shin, J. M. Headrick, E. G. Diken, J. R. Roscioli, G. H. Weddle, and M. A. Johnson, Science **306**, 675 (2004).
[17] N. I. Hammer, J. R. Roscioli, and M. A. Johnson, J. Phys. Chem. A **109**, 7896 (2005).
[18] N. I. Hammer, J. R. Roscioli, J. C. Bopp, J. M. Headrick, and M. A. Johnson, J. Chem. Phys. **123**, 244311 (2005).
[19] J. R. Roscioli, N. I. Hammer, M. A. Johnson, K. Diri, and K. D. Jordan, J. Chem. Phys. **128**, 104314 (2008).
[20] A. E. Bragg, J. R. R. Verlet, A. Kammrath, O. Cheshnovsky, and D. M. Neumark, Science **306**, 669 (2004).
[21] J. R. R. Verlet, A. E. Bragg, A. Kammrath, O. Cheshnovsky, and D. M. Neumark, Science **307**, 93 (2005).
[22] A. E. Bragg, J. R. R. Verlet, A. Kammrath, O. Cheshnovsky, and D. M. Neumark, J. Am. Chem. Soc. **127**, 15283 (2005).
[23] K. R. Asmis, G. Santabrogio, J. Zhou, E. Garand, J. Headrick, D. Goebbert, M. A. Johnson, and D. M. Neumark, J. Chem. Phys. **126**, 191105 (2007).

[24] G. B. Griffin, R. M. Young, O. T. Ehrler, and D. M. Neumark, J. Chem. Phys. **131**, 194302 (2009).
[25] D. H. Paik, I. Lee, D. Yang, J. Baskin, and A. H. Zewail, Science **306**, 672 (2004).
[26] D. M. Bartels, K. Takahashi, J. A. Cline, T. W. Marin, and C. D. Jonah, J. Phys. Chem. A **109**, 1299 (2005).
[27] Y. Du, E. Price, and D. M. Bartels, Chem. Phys. Lett. **438**, 234 (2007).
[28] L. Ma, K. Majer, F. Chirot, and B. von Issendorff, J. Chem. Phys. **131**, 144303 (2009).
[29] P. M. Hare, E. A. Price, C. M. Stanisky, I. Janik, and D. M. Bartels, J. Phys. Chem. A **114**, 1766 (2010).
[30] Y. Tang, H. Shen, K. Sekiguchi, N. Kurahashi, T. Mizuno, Y. I. Suzuki, and T. Suzuki, Phys. Chem. Chem. Phys. **12**, 3653 (2010).
[31] K. R. Siefermann, Y. Liu, E. Lugovoy, O. Link, U. Buck, B. Winter, and B. Abel, Nat. Chem. **2**, 274 (2010).
[32] A. T. Shreve, T. A. Yen, and D. M. Neumark, Chem. Phys. Lett. **493**, 216 (2010).
[33] A. Wallqvist, D. Thirumalai, and B. J. Berne, J. Chem. Phys. **85**, 1583 (1986).
[34] A. Wallqvist, D. Thirumalai, and B. J. Berne, J. Chem. Phys. **86**, 6404 (1987).
[35] A. Wallqvist, G. Martyna, and B. J. Berne, J. Phys. Chem. **92**, 1721 (1988).
[36] R. N. Barnett, U. Landman, and C. L. Cleveland, Phys. Rev. Lett. **59**, 811 (1987).
[37] R. N. Barnett, U. Landman, C. L. Cleveland, and J. Jortner, J. Chem. Phys. **88**, 4429 (1988).
[38] R. N. Barnett, U. Landman, D. Scharf, and J. Jortner, Acc. Chem. Res. **22**, 350 (1989).
[39] J. Schnitker and P. J. Rossky, J. Chem. Phys. **86**, 3471 (1987).
[40] P. J. Rossky and J. Schnitker, J. Phys. Chem. **92**, 4277 (1988).
[41] J. Schnitker, K. Motakabbir, P. J. Rossky, and R. A. Friesner, Phys. Rev. Lett. **60**, 456 (1988).
[42] B. J. Schwartz and P. J. Rossky, J. Phys. Chem. **98**, 4489 (1994).
[43] B. J. Schwartz and P. J. Rossky, J. Chem. Phys. **101**, 6902 (1994).
[44] B. J. Schwartz and P. J. Rossky, J. Chem. Phys. **101**, 6917 (1994).
[45] B. J. Schwartz and P. J. Rossky, Phys. Rev. Lett. **72**, 3282 (1994).
[46] A. Staib and D. Borgis, J. Chem. Phys. **103**, 2642 (1995).
[47] L. Turi and D. Borgis, J. Chem. Phys. **117**, 6186 (2002).
[48] L. Turi, W.-S. Sheu, and P. J. Rossky, Science **309**, 914 (2005).
[49] L. Turi, Á. Madarász, and P. J. Rossky, J. Chem. Phys. **125**, 014308 (2006).
[50] D. Borgis, P. J. Rossky, and L. Turi, J. Chem. Phys. **125**, 064501 (2006).
[51] D. Borgis, P. J. Rossky, and L. Turi, J. Chem. Phys. **127**, 174508 (2007).
[52] Á. Madarász, P. J. Rossky, and L. Turi, J. Chem. Phys. **126**, 234707 (2007).
[53] A. Madarász, P. J. Rossky, and L. Turi, J. Chem. Phys. **130**, 124319 (2009).
[54] L. Turi, G. Hantal, P. J. Rossky, and D. Borgis, J. Chem. Phys. **131**, 024119 (2009).
[55] I. Park, K. Cho, S. Lee, K. S. Kim, and J. D. Joannopoulos, Comput. Mater. Sci. **21**, 291 (2001).
[56] F. Wang and K. D. Jordan, J. Chem. Phys. **119**, 11645 (2003).
[57] A. DeFusco, T. Sommerfeld, and K. D. Jordan, Chem. Phys. Lett. **455**, 135 (2008).
[58] M. Boero, M. Parrinello, K. Terakura, T. Ikeshoji, and C. C. Liew, Phys. Rev. Lett. **90**, 226403 (2003).
[59] J. M. Herbert and M. Head-Gordon, J. Am. Chem. Soc. **128**, 13932 (2006).
[60] J. M. Herbert and M. Head-Gordon, Proc. Natl. Acad. Sci. U.S.A. **103**, 14282 (2006).
[61] I. A. Shkrob, J. Phys. Chem. A **111**, 5223 (2007).
[62] I. A. Shkrob, W. J. Glover, R. E. Larsen, and B. J. Schwartz, J. Phys. Chem. A **111**, 5232 (2007).
[63] K. A. Tay and A. Boutin, J. Phys. Chem. B **113**, 11943 (2009).
[64] L. D. Jacobson and J. M. Herbert, J. Am. Chem. Soc. **132**, 10000 (2010).
[65] R. E. Larsen, W. J. Glover, and B. J. Schwartz, Science **329**, 65 (2010).
[66] J. V. Coe, S. M. Williams, and K. H. Bowen, Int. Rev. Phys. Chem. **27**, 27 (2008).
[67] D. M. Bartels, J. Chem. Phys. **115**, 4404 (2001).
[68] J. R. R. Verlet, A. E. Bragg, A. Kammrath, O. Cheshnovsky, and D. M. Neumark, Science **310**, 1769 (2005).
[69] L. Turi, W.-S. Sheu, and P. J. Rossky, Science **310**, 1769 (2005).
[70] E. J. Hart and M. Anbar, *The Hydrated Electron* (Wiley-Interscience, New York, 1970).
[71] R. Lugo and P. Delahay, J. Chem. Phys. **57**, 2122 (1972).
[72] F.-Y. Jou and G. R. Freeman, J. Phys. Chem. **81**, 909 (1977).
[73] F.-Y. Jou and G. R. Freeman, Can. J. Chem. **57**, 591 (1979).
[74] H. J. C. Berendsen, J. P. M. Postma, W. F. van Gunsteren, and J. Hermans, in *Intermolecular Forces*, edited by B. Pullman (Reidel, Dordrecht, 1981), p. 331.
[75] K. Toukan and A. Rahman, Phys. Rev. B **31**, 2643 (1985).
[76] J. M. Herbert, L. D. Jacobson, and C. F. Williams, in *Molecular Potential Energy Surfaces in Many Dimensions*, edited by M. M. Law and A. Ernesti (Collaborative Computational Project on Molecular Quantum Dynamics, Daresbury, United Kingdom, 2009), pp. 28–38.
[77] J. M. Herbert and L. D. Jacobson, "Nature's most squishy ion: The important role of solvent polarization in the description of the hydrated electron," Int. Rev. Phys. Chem. (in press).
[78] C. F. Williams and J. M. Herbert, J. Phys. Chem. A **112**, 6171 (2008).
[79] L. D. Jacobson, C. F. Williams, and J. M. Herbert, J. Chem. Phys. **130**, 124115 (2009).
[80] P. Ren and J. W. Ponder, J. Phys. Chem. B **107**, 5933 (2003).
[81] P. Ren and J. W. Ponder, J. Phys. Chem. B **108**, 13427 (2004).
[82] A. Gaathon, G. Czapski, and J. Jortner, J. Chem. Phys. **58**, 2648 (1973).
[83] J. M. Herbert and M. Head-Gordon, J. Phys. Chem. A **109**, 5217 (2005).
[84] M. A. Morrison and L. A. Collins, Phys. Rev. B **17**, 918 (1978).
[85] J. Schnitker and P. J. Rossky, J. Chem. Phys. **86**, 3462 (1987).
[86] L. Turi, M.-P. Gaigeot, N. Levy, and D. Borgis, J. Chem. Phys. **114**, 7805 (2001).
[87] R. N. Barnett, U. Landman, C. L. Cleveland, and J. Jortner, J. Chem. Phys. **88**, 4421 (1988).
[88] C. J. Smallwood, R. E. Larsen, W. J. Glover, and B. J. Schwartz, J. Chem. Phys. **125**, 074102 (2006).
[89] J. C. Phillips and L. Kleinman, Phys. Rev. **116**, 287 (1959).
[90] T. Tsuneda, T. Suzumura, and K. Hirao, J. Chem. Phys. **110**, 10664 (1999).
[91] H. Iikura, T. Tsuneda, T. Yanai, and K. Hirao, J. Chem. Phys. **115**, 3540 (2001).
[92] K. Yagi, Y. Okano, Y. Kawashima, T. Tsudeda, and K. Hirao, J. Phys. Chem. A **112**, 9845 (2008).
[93] B. Thole, Chem. Phys. **59**, 341 (1981).
[94] F. Wang and K. D. Jordan, J. Chem. Phys. **116**, 6973 (2002).
[95] Y. Shao, L. Fusti-Molnar, Y. Jung, J. Kussmann, C. Ochsenfeld, S. T. Brown, A. T. B. Gilbert, L. V. Slipchenko, S. V. Levchenko, D. P. O'Neill, R. A. DiStasio, Jr., R. C. Lochan, T. Wang, G. J. O. Beran, N. A. Besley, J. M. Herbert, C. Y. Lin, T. Van Voorhis, S. H. Chien, A. Sodt, R. P. Steele, V. A. Rassolov, P. E. Maslen, P. P. Korambath, R. D. Adamson, B. Austin, J. Baker, E. F. C. Byrd, H. Dachsel, R. J. Doerksen, A. Dreuw, B. D. Dunietz, A. D. Dutoi, T. R. Furlani, S. R. Gwaltney, A. Heyden, S. Hirata, C.-P. Hsu, G. Kedziora, R. Z. Khalliulin, P. Klunzinger, A. M. Lee, M. S. Lee, W. Liang, I. Lotan, N. Nair, B. Peters, E. I. Proynov, P. A. Pieniazek, Y. M. Rhee, J. Ritchie, E. Rosta, C. D. Sherrill, A. C. Simmonett, J. E. Subotnik, H. L. Woodcock III, W. Zhang, A. T. Bell, A. K. Chakraborty, D. M. Chipman, F. J. Keil, A. Warshel, W. J. Hehre, H. F. Schaefer III, J. Kong, A. I. Krylov, P. M. W. Gill, and M. Head-Gordon, Phys. Chem. Chem. Phys. **8**, 3172 (2006).
[96] See supplementary material at http://dx.doi.org/10.1063/1.3490479 for the fitting parameters that define the pseudopotential, along with additional benchmark data.
[97] L. Mones and L. Turi, J. Chem. Phys. **132**, 154507 (2010).
[98] C. W. Murray, S. C. Racine, and E. R. Davidson, J. Comput. Phys. **103**, 382 (1992).
[99] TINKER, Version 4.2, http://dasher.wustl.edu/tinker.
[100] G. Martyna, M. Tuckerman, D. Tobias, and M. Klein, Mol. Phys. **87**, 1117 (1996).
[101] D. Frenkel and B. Smit, *Understanding Molecular Simulation: From Algorithms to Applications* (Academic, San Diego, 2002).
[102] J. V. Coe, S. T. Arnold, J. G. Eaton, G. H. Lee, and K. H. Bowen, J. Phys. Chem. **125**, 014315 (2006).
[103] J. M. Herbert and M. Head-Gordon, Phys. Chem. Chem. Phys. **8**, 68 (2006).
[104] J. Xu and K. D. Jordan, J. Phys. Chem. A **114**, 1364 (2010).
[105] P. Wernet, D. Nordlund, U. Bergmann, M. Cavalleri, H. Ogasawara, L. A. Naslund, T. K. Hirsch, L. Ojamae, P. Glatzel, L. G. M. Petterson, and A. Nilsson, Science **304**, 995 (2004).
[106] J. D. Louck and H. W. Galbraith, Rev. Mod. Phys. **48**, 69 (1976).

[107] M. Maroncelli and G. R. Fleming, J. Chem. Phys. **89**, 5044 (1988).
[108] M. Leslie and M. J. Gillan, J. Phys. C **18**, 973 (1985).
[109] G. Makov and M. C. Payne, Phys. Rev. B **51**, 4014 (1995).
[110] G. Makov and A. Nitzan, J. Phys. Chem. **98**, 3459 (1994).
[111] Within a spherical cavity model, the $1s \rightarrow 1p$ transitions carry essentially all of the oscillator strength, since the $1s \rightarrow 2s$ and $1s \rightarrow 1d$ transitions are dipole-forbidden, while the $2p$ states are quite diffuse and have little overlap with the $1s$ ground state, for cavity radii and binding energies consistent with e^-_{aq}.
[112] M. C. Cavanagh, I. B. Martini, and B. J. Schwartz, Chem. Phys. Lett. **396**, 359 (2004).
[113] P. J. Reid, C. Silva, P. K. Walhout, and P. F. Barbara, Chem. Phys. Lett. **228**, 658 (1994).
[114] M. Assel, R. Laenen, and A. Laubereau, J. Phys. Chem. A **102**, 2256 (1998).
[115] M. Assel, R. Laenen, and A. Laubereau, J. Chem. Phys. **111**, 6869 (1999).
[116] I. A. Shkrob, Chem. Phys. Lett. **467**, 84 (2008).